PHILOSOPHICAL TRANSACTIONS OF THE ROYAL SOCIETY B

rstb.royalsocietypublishing.org

Research

Cite this article: Grossberg S, Pilly PK. 2014 Coordinated learning of grid cell and place cell spatial and temporal properties: multiple scales, attention and oscillations. *Phil. Trans. R. Soc. B* **369**: 20120524.
http://dx.doi.org/10.1098/rstb.2012.0524

One contribution of 24 to a Theo Murphy Meeting Issue 'Space in the brain: cells, circuits, codes and cognition'.

Subject Areas:
behaviour, computational biology, neuroscience, theoretical biology

Keywords:
grid cells, place cells, self-organizing map, spatial navigation, attention, adaptive timing

Author for correspondence:
Stephen Grossberg
e-mail: steve@bu.edu

†These authors contributed equally to this study.
‡Present address: Center for Neural and Emergent Systems, Information and Systems Sciences Laboratory, HRL Laboratories, 3011 Malibu Canyon Road, Malibu, CA 90265, USA.

Royal Society Publishing

Coordinated learning of grid cell and place cell spatial and temporal properties: multiple scales, attention and oscillations

Stephen Grossberg† and Praveen K. Pilly†,‡

Department of Mathematics, Center for Adaptive Systems, Graduate Program in Cognitive and Neural Systems, Center for Computational Neuroscience and Neural Technology, Department of Mathematics, Boston University, 677 Beacon Street, Boston, MA 02215, USA

A neural model proposes how entorhinal grid cells and hippocampal place cells may develop as spatial categories in a hierarchy of self-organizing maps (SOMs). The model responds to realistic rat navigational trajectories by learning both grid cells with hexagonal grid firing fields of multiple spatial scales, and place cells with one or more firing fields, that match neurophysiological data about their development in juvenile rats. Both grid and place cells can develop by detecting, learning and remembering the most frequent and energetic co-occurrences of their inputs. The model's parsimonious properties include: similar ring attractor mechanisms process linear and angular path integration inputs that drive map learning; the same SOM mechanisms can learn grid cell and place cell receptive fields; and the learning of the dorsoventral organization of multiple spatial scale modules through medial entorhinal cortex to hippocampus (HC) may use mechanisms homologous to those for temporal learning through lateral entorhinal cortex to HC ('neural relativity'). The model clarifies how top-down HC-to-entorhinal attentional mechanisms may stabilize map learning, simulates how hippocampal inactivation may disrupt grid cells, and explains data about theta, beta and gamma oscillations. The article also compares the three main types of grid cell models in the light of recent data.

1. Introduction

The hippocampus (HC) and medial entorhinal cortex (MEC) are critical brain areas for spatial learning, memory and behaviour [1–3]. Place cells in HC fire whenever the rat is positioned in a specific localized region, or 'place', of an environment [4], and also exhibit multiple firing fields in large spaces [5–7]. Different place cells prefer different regions, and the place cell ensemble code enables the animal to localize itself in an environment.

Since the work of O'Keefe & Dostrovsky [4], research on place cells has disclosed that they receive two kinds of inputs: one conveying information about the sensory context experienced from a given place, and the other from a navigational, or path integration, system that tracks relative position in the world by integrating self-movement angular and linear velocity estimates for instantaneous rotation and translation, respectively. An important open problem is to explain how sensory context and path integration information are combined in the control of navigation (see [8–10]). This article focuses upon a model of how path integration information is represented by MEC grid cells and HC place cells.

Grid cells in superficial layers of MEC fire in multiple places that may form a regular hexagonal grid across the navigable environment [11]. The primary determinants of grid cell firing are path integration-based inputs [12]. Indeed, the environmental signals sensed at each of the various hexagonally distributed spatial firing positions of a single grid cell are different. The ensemble of entorhinal grid cells may, from their location one synapse upstream of hippocampal CA1 and CA3 place cells, represent the main processed output of this path integration system.

The spatial fields of grid cells recorded from a given dorsoventral location in rat MEC exhibit different phases; that is, they are offset from each other [11]. In addition, the spacing between neighbouring fields and the field sizes of grid cells increases, on average, from the dorsal to the ventral end of the MEC [13–15]. These properties have led to the suggestion that a place cell with spatial selectivity for a given position may be derived by selectively combining grid cells with multiple spatial phases and scales that are coactive at that position, in such a way that the grid-to-place transformation allows for the expansion of the scale of spatial representation in the brain [12,16,17]. In other words, the maximal size of the environment in which a place cell exhibits only a single firing field can be much larger than the individual scales of grid cells that are combined to fire the place cell. Models have been proposed in which place fields in one-dimensional and two-dimensional spaces are learned based on inputs from hard-wired grid cells of multiple spatial scales and phases [17–20].

Each of the sections below summarizes an accomplishment of the model along with pertinent neurobiological data. Sections 2 and 3 propose how grid cells and place cells may arise during development through a learning process that uses the same self-organizing map (SOM) laws for learning both types of cells. SOM laws have been used to explain data about many other kinds of learned maps in the brain, notably maps that arise during development for vision, audition and cognition. The current results suggest that specializations of SOM dynamics also play a key role in spatial coding and navigation. Section 4 notes that the model's properties are obtained using either rate-based or spiking neurons, and that new properties, such as theta band modulation, also arise in the spiking model. Sections 5 and 6 propose how the model may learn the observed gradient of grid cell spatial scales along the dorsoventral axis of the MEC, and how distinct grid cell modules and different frequencies of subthreshold membrane potential oscillations (MPOs) may arise through this developmental process. Section 7 suggests that the gradient of spatial scales that arises through the MEC and its hippocampal projections to place cells may use neural mechanisms that are homologous to those that create the observed gradient of temporal scales through the lateral entorhinal cortex (LEC) and its hippocampal projections to 'time cells'. In both cases, a spectrum of small scales, whether spatial or temporal, gives rise to larger scales that can represent spatial or temporal properties of observable behaviours. Section 8 notes another parsimonious property of the model; namely how both angular velocity and linear velocity path integration inputs may be processed by similar ring attractor circuits. Without further mechanisms, the above learning processes could become unstable in response to ever-changing series of inputs through time; in particular, grid and place fields could drift and become spatially non-specific. Sections 9 and 10 propose how top-down attentional matching mechanisms from CA1 to MEC may dynamically stabilize the learned grid and place cells, and how top-down matches (mismatches) may cause gamma (beta) oscillations. Sections 11 and 12 summarize model explanations of how inactivating medial septum (MS) or top-down inputs from the HC to the MEC may cause adverse effects on grid cell firing. Section 12 also compares the SOM model with the oscillatory interference and continuous attractor models of grid cells.

2. How do grid cells and place cells arise through development and learning?

The GridPlaceMap neural model and its variants [17,21–25] show how grid cells and place cells may develop in a hierarchy of SOMs (figure 1). The modern equations for a SOM were introduced by [26,27] in response to an earlier version of the model by von der Malsburg [28]. In such a SOM, input patterns are processed by an adaptive filter. The filtered inputs activate a recurrent competitive network whose lateral inhibitory interactions choose the maximally activated cell (population), or a small number of the most highly activated cells. The winning cells trigger learning in the adaptive weights that exist at the synapses of the adaptive filter pathways which end at those cells. The adaptive weights learn a normalized time-average of the inputs that they receive during the time intervals when their target cell wins the competition. There is, thus, a conservation of total synaptic weight to each map cell by homeostatic competitive interactions among incoming axons (see equations (A 6) and (B 6)), consistent with data of Royer & Pare [29]. In this way, the vector of adaptive weights to each cell in the map becomes tuned to the statistics of the inputs that enabled it to win the competition. The SOM can hereby more strongly activate each winning cell in response to these and similar inputs in the future. Each such cell becomes a *category*, or compressed representation, of the inputs that are able to activate it.

In the GridPlaceMap model, two successive SOMs exist, wherein the first SOM is activated by pre-processed path integration inputs, and the second SOM is activated by output signals from the first SOM (figure 1). The grid cells and place cells are learned as spatial categories in their respective SOMs. The model converts realistic rat navigational trajectories into the path integration inputs that trigger learning of grid cells with hexagonal grid firing fields of multiple spatial scales, and place cells with one or more firing fields. Place cells can represent positions in much larger spaces than grid cells, which enable them to support useful navigational behaviours.

The properties of these model cells match neurophysiological data about the corresponding cells *in vivo* and their development in juvenile rats [23]. Neurophysiological data that the model simulates include the distributed spatial phases of place fields and grid fields, similar grid orientations for similar grid scales [11,15], and multi-modal firing fields of place cells in large spaces [5–7]. Simulated developmental data about grid cells include changes in gridness score and grid spacing during early spatial experience, and simulated developmental data about place cells include changes in spatial information and inter-trial stability measures [30,31].

3. Homologous self-organizing map laws for grid and place cell learning: recurrent inhibition

Remarkably, all these data are emergent, or interactive, properties of grid cells and place cells that are learned in a hierarchy of SOMs wherein each SOM in the hierarchy obeys the same laws. Specializations of these laws have successfully modelled multiple parts of the brain, notably visual cortical map

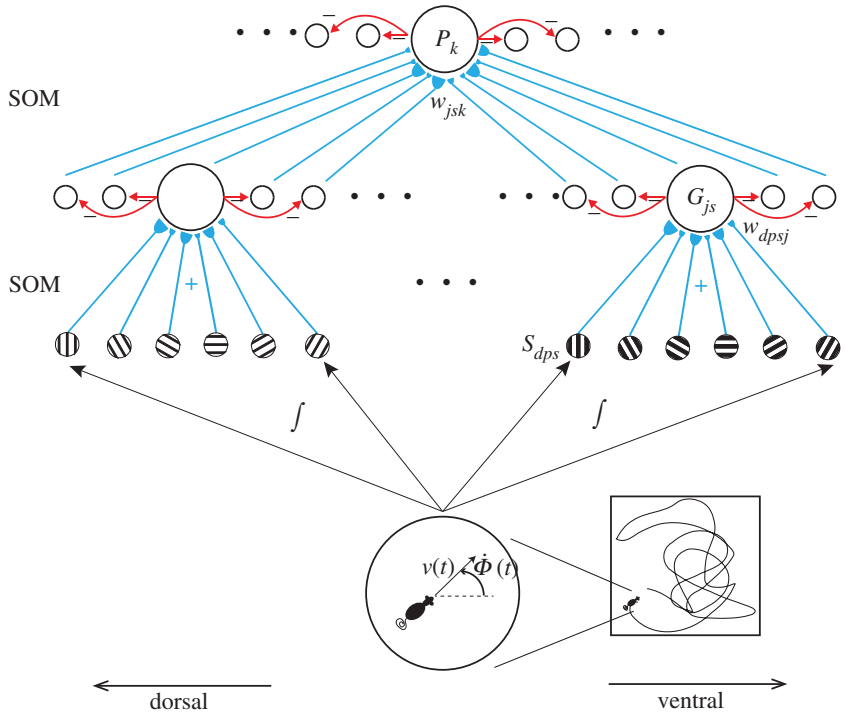

Figure 1. GridPlaceMap self-organizing map hierarchy of grid and place cell activation and learning [23,25]: stripe cells in either the parasubiculum (PaS) or the deeper layers of medial entorhinal cortex (MEC), self-organizing grid cells in layer II of MEC and self-organizing place cells in hippocampal area CA3 learn to represent position in increasingly large spaces based on internally generated signals corresponding to translational and rotational movements during navigation. Reproduced with permission from Pilly & Grossberg [23].

development [32–34]. Each SOM amplifies and learns to categorize the most frequent and energetic co-occurrences of its inputs [23], while suppressing the representation of less frequent and energetic input patterns using its recurrent inhibitory interactions.

The different grid cell and place cell receptive field properties emerge because they experience different input sources. The place cells learn from the developing grid cells of multiple scales that input to them. The grid cells learn from stripe cells that input to them. Stripe cells are selective for allocentric direction, spatial scale and spatial phase (figure 2). Each stripe cell represents displacement from a reference position by integrating the linear velocity of the navigator. Stripe cells are organized into ring attractors. All the stripe cells in a given ring attractor are tuned to movement along the same direction. Because of their different positions in the ring attractor, different stripe cells fire at different spatial phases. An activity bump that represents directional displacement cycles around the ring attractor as the animal moves. One complete cycle of the bump around the ring attractor activates the same stripe cell again. This distance determines the spatial scale of stripe cells in that ring attractor. The name 'stripe cell' describes the periodic directionally selective activations of stripe cells as the environment is navigated. The parallel activations of multiple stripe cell ring attractors, each selective to a different spatial scale and directional preference, implicitly represent the animal's position in the environment.

The analogous concept of 'band cells' was introduced in Burgess *et al.* [35]. Band cells, however, operate by a mechanism of oscillatory interference between a baseline oscillation and an oscillation with a velocity-modulated frequency, which plays no role in the SOM model. A band cell is more similar to a stripe cell when the baseline oscillation has a zero frequency, but then the corresponding oscillatory interference models of grid cells [35,36] lose most of their explanatory properties, including theta band modulation [30,31] and theta phase precession [37].

Each SOM in the model has the property that, among all the input patterns to which it is exposed through time, the ones to which its map cells gradually become tuned by learning are those that comprise greater numbers of coactive input cells *and* are more often encountered as the animal navigates through space. In other words, each SOM model learns from its most energetic and frequent input patterns. This occurs, in part, because learning is gated by postsynaptic activity of winner map cell(s), which is larger when more input cells are simultaneously active to make the total input more 'energetic'; and, in part, because learning occurs at a slow enough time-scale to be sensitive to the most 'frequent' of the successful input patterns.

Hexagonal grids are learned in the model owing to a property of the trigonometry of spatial navigation to which the SOM dynamics are sensitive. This property was first described in [22], and refined in [23]. It controls the sets of coactive stripe cells, for a given spatial scale, that the grid cell layer experiences as the space is traversed. As noted above, the entorhinal SOM detects and learns grid cell firing patterns in response to the most energetic and frequent coactivations of these stripe cell sets through time, while suppressing less energetic and frequent coactivations using the recurrent inhibitory interactions among map cells. The receptive fields of these inhibitory interactions are chosen to be isotropic across space.

Owing to this trigonometric property, sets of coincident inputs from three stripe cells whose preferred directions differ by 60° are almost the most frequent combinations of inputs through time. Inputs from two stripe cells that differ by 90° are slightly more frequent, because an arbitrary stripe cell persists in its activity if the animal moves along

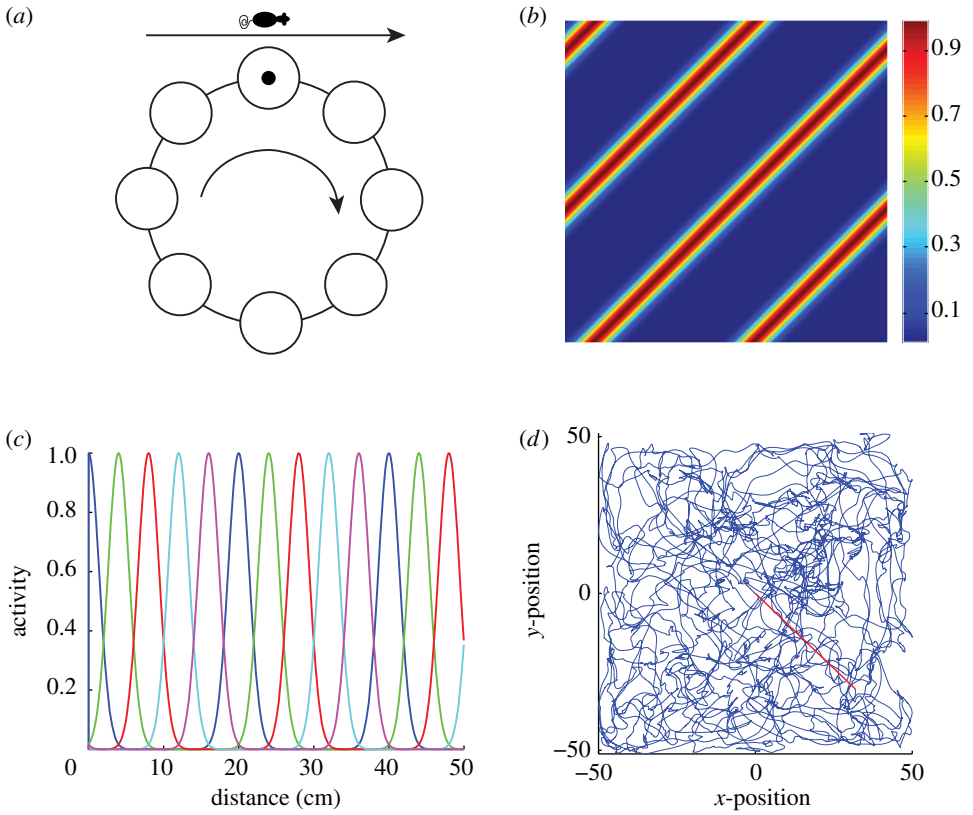

Figure 2. Linear velocity path integration. (*a*) Ring attractor neural circuit for linear velocity path integration in which translational movements control the movement of an activity bump along the ring. (*b*) Firing rate map of an idealized stripe cell with a spacing of 35 cm and whose fields are oriented at 45°. This stripe cell is responsive to translational movement with a component along either 135° or its opponent direction −45°. (*c*) Activities of stripe cells of a given spacing (20 cm) but five different spatial phases (see colours) as a function of displacement from the origin along their preferred direction. (*d*) Real rat trajectory [13] of approximately 10 min in a 100 × 100 cm environment used in training the model. Reproduced with permission from Pilly & Grossberg [23].

90° from its preferred direction. However, the total sizes of the input coactivations by three stripe cells separated by 60° are larger, or more energetic, than coactivations by two stripe cells separated by 90°, so that the 60° configurations win the competition through time, and cause the observed hexagonal receptive fields of grid cells to be learned, as the model is stimulated by realistic navigational trajectories in an open field. Along the same lines, the typically unimodal firing fields of place cells emerge in the hippocampal SOM in response to sets of coactive grid cells of multiple scales at various positions that are frequently visited.

The key role of recurrent inhibitory interactions among grid cells is consistent with experimental evidence [38,39]. Continuous attractor models also use recurrent inhibitory interactions, but they embody some problematic computational hypotheses, including the need for recurrent inhibitory interactions with specific directional asymmetries, which differ significantly from those of the SOM model, wherein global isotropic inhibition has sufficed to learn the properties summarized above (see §12).

In the GridPlaceMap model, place cells learn only by receiving inputs from grid cells. It has also been reported that some place cells may occur before vigorous grid cell development is initiated during development [30,31]. There are several possible reasons for this, including the fact that place cells can respond to both visual and path integration inputs [10]. The GridPlaceMap model and place cell learning models before it [17] suggest that place cells with the largest possible spatial scales (i.e. with greater spatial information in larger spaces) may develop from grid cell inputs with multiple spatial scales, indeed with place cell spatial scales that can be as large as the least common multiple of the grid cell scales which drive them.

4. Rate-based and spiking models

Grid and place cell learning can occur in SOM models that are built up from either rate-based or spiking neurons. The sGridPlaceMap model using spiking neurons [25] builds upon the rate-based model of grid and place cell learning described above [23], and illustrates a general method for converting rate-based adaptive neural models into models whose cells obey spiking dynamics. This method has also been used to convert a rate-based model of three-dimensional vision into a spiking model [40]. The sGridPlaceMap model, which incorporates AMPA-, NMDA- and $GABA_A$-mediated ion channels, replicates all the key properties of the data (see §2 and figures 3 and 4). This is possible, because the activity-dependent SOM learning law (see equation (A 6)) can work just as well when presynaptic and postsynaptic activities are replaced by exponentially decaying trace variables that track the spikes of the pertinent neurons (see equation (B 13)). New properties also emerge in the spiking model, including the appearance of theta band modulation of spike times in a subset of learned grid and place cells [30,31]. MATLAB code to implement the spiking model [25] is available at: https://senselab.med.yale.edu/modeldb/ShowModel.asp?model=148035.

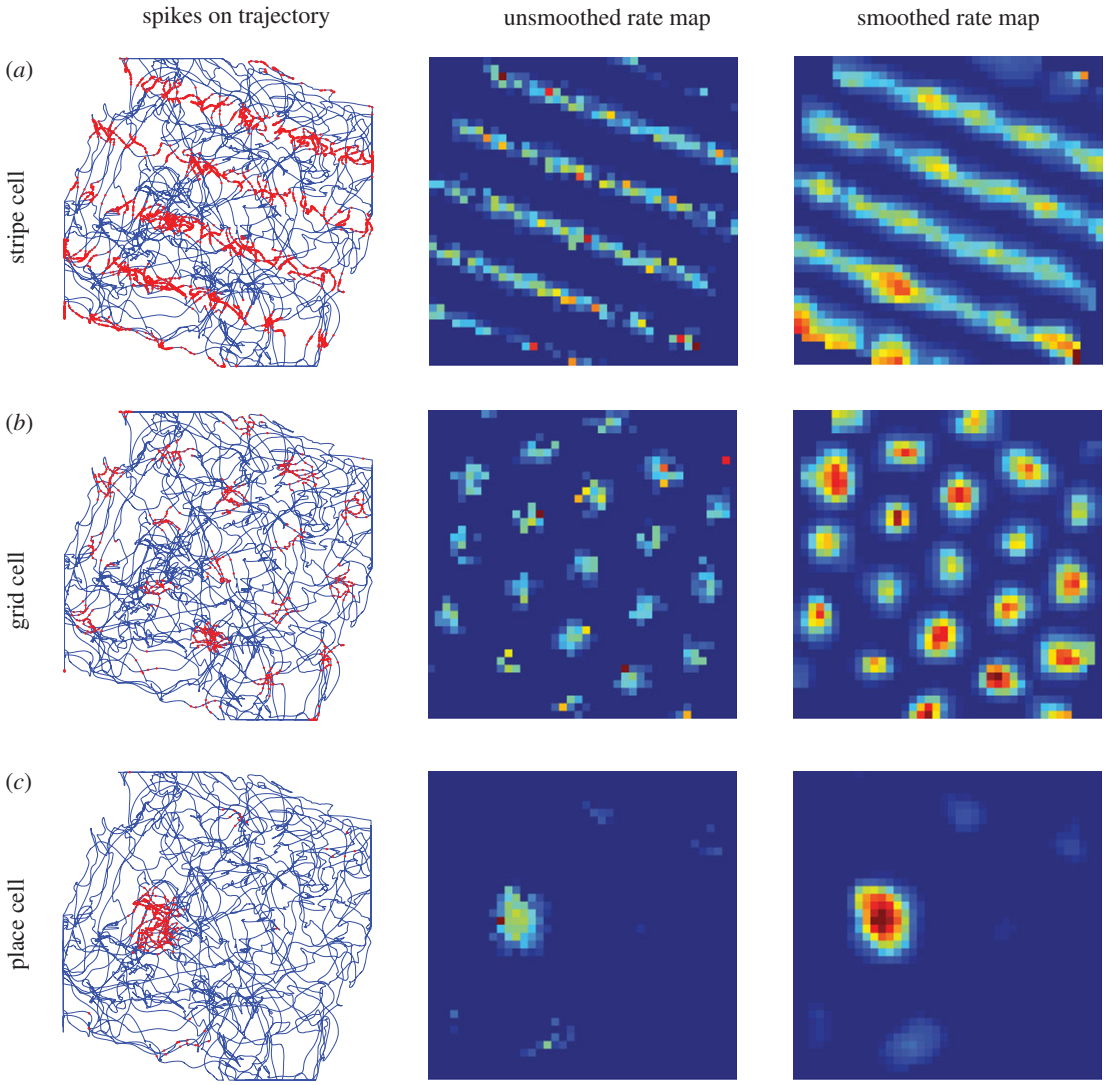

Figure 3. Different spatial cell types in the parahippocampal-hippocampal system. Spatial responses of representative (*a*) stripe, (*b*) grid and (*c*) place cells in the spiking SOM model [25]. The first column shows the spike locations (red dots) of the cells superimposed on the trajectory of the animal during a trial. The second and third columns show the unsmoothed and smoothed spatial rate maps, respectively, of the cells. Colour coding from blue (min.) to red (max.) is used for each rate map. Reproduced with permission from Pilly & Grossberg [25].

5. Learning the dorsoventral gradient of grid cell scales and oscillation frequencies

Both the spatial and temporal properties of grid cells vary along the dorsoventral axis of MEC. *In vitro* recordings of medial entorhinal layer II stellate cells have revealed subthreshold MPOs whose temporal periods, and the time constants of excitatory postsynaptic potentials (EPSPs), both tend to increase along this axis [41–44]. Slower (faster) subthreshold MPOs and slower (faster) EPSPs correlate with larger (smaller) grid spacings and field widths. Individual grid cells face the 'scale selection problem' to sample and learn hexagonal grid exemplars of a particular spatial scale when adaptive inputs from stripe cells of multiple scales initially converge on them. The SOM model [21] demonstrates that the anatomical gradient of increasing grid spatial scales [14] can be learned by cells that respond more slowly along the dorsoventral axis (see μ in equation (A 5)) [42] to their inputs from stripe cells of multiple scales, while adapting to them and undergoing refraction. The model cells also exhibit MPOs with frequencies that covary with their response rates in response to steady current injections (figure 5). The gradient in intrinsic rhythmicity is thus not compelling evidence for oscillatory interference as a mechanism of grid cell firing (cf. [35,36]). Consistent with this, a recent study using HCN1 knockout mice reported that the development of the grid scale gradient is not dependent on the presence of the gradient in intrinsic oscillation frequency [45].

6. Development of grid cell modules

Grid cells along the dorsoventral axis were shown in [15, p. 72] to 'cluster into a small number of layer-spanning anatomically overlapping modules with distinct scale, orientation, asymmetry and theta-frequency modulation'. These grid cell modules are distributed across wide regions along the dorsoventral axis with substantial overlaps among the different clusters (figure 6*a*).

If indeed grid cells develop from path integration inputs that are mediated by stripe, or band, cells, then the data of [15] imply that the problem of selecting from multiple scales of stripe cells during development is a real one,

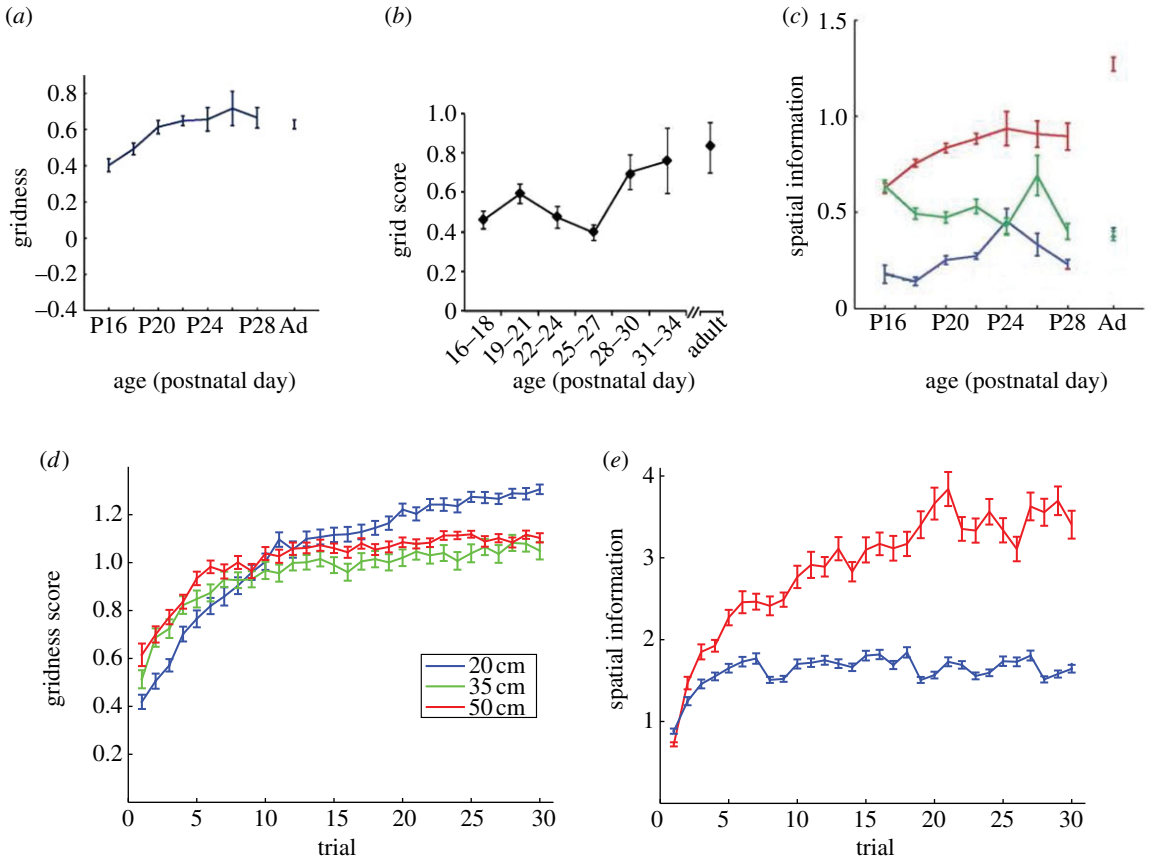

Figure 4. Development of grid and place cells in juvenile rats. (*a–c*) Data from juvenile rats and (*d,e*) spiking SOM model simulations [25] regarding the changes in gridness score of grid cells (*a*: [31]; *b*: [30]; *d*: model), and in spatial information of grid and place cells (*c*: [31]; *e*: model), during the postnatal development period. (*d*) Shows simulation results for each input stripe spacing. Blue and red curves in (*c,e*) correspond to grid and place cells, respectively. Results for model grid cells shown in (*e*) are averaged across the three stripe spacings. Error bars correspond to standard error of mean. Data reproduced with permission from [30] and [31]. Simulations reproduced with permission from [25].

because a simple topographic mapping from stripe cells to grid cells of individual scales is not consistent with these data. Preliminary simulations (figure 6*b–g*) using the SOM model [21] demonstrate the development of multiple grid scales (up to three) within the same self-organizing local network of map cells that recurrently inhibit each other and vary in their response rates μ (see equation (A 5)). Model simulations are consistent with experiments showing spreads in intrinsic properties of MEC layer II stellate cells at the same dorsoventral locations [41,42,46,47]. The SOM equations and parameters that were used in the module simulations are provided in appendix A. Future work will attempt to simulate more properties.

7. Homologous spatial and temporal mechanisms: neural relativity

This spatial gradient mechanism is homologous to a gradient mechanism for temporal learning in the LEC and its hippocampal projections that has been modelled earlier [48–50]. Both the spatial learning and temporal learning models propose how a gradient, or 'spectrum', of response rates controls the emergence of encoding at multiple scales. In the temporal learning model, cells respond maximally in different, but overlapping, time intervals. As a result, these cells learn maximally in different time intervals. Such learning occurs when the cell is active at a time when a learning signal is also active. The output signals of cells that respond faster are active for shorter time intervals than the output signals of cells that respond more slowly, a property that is called the Weber law. The outputs of all these cells are multiplied, or gated, by their learned weights before being added together at cells that can represent longer time intervals than any of their constituent input cells. Indeed, these output cells can bridge behaviourally relevant time-scales in the hundreds of milliseconds. This model of adaptively timed learning is thus called the *spectral timing* model.

Correspondingly, the SOM model shows how the dorsoventral gradient in response rates develops a spectrum of grid cell scales. It is thus called the *spectral spacing* model [21]. As in the spectral timing model, in the spectral spacing model, multiple entorhinal grid cell scales are combined to give rise to hippocampal place cells that can represent larger spaces than can an individual grid cell.

The spectral timing model has been used to explain and simulate data about the role of HC in learning behaviours that bridge temporal gaps, such as occurs during trace conditioning and delayed matching-to-sample, in both normal individuals and amnesics [48–50]. As noted above, spectrally timed learning has Weber law properties such that larger inter-stimulus intervals between unconditioned and conditioned stimuli lead to learned response curves with broader variances, a property that is also called 'scalar timing' [51–54]. Hippocampal 'time cells' with all the properties required to achieve spectral timing, including the Weber law, have been recently reported [55, p. 738]; in particular, '... the mean peak firing rate for each time cell occurred at

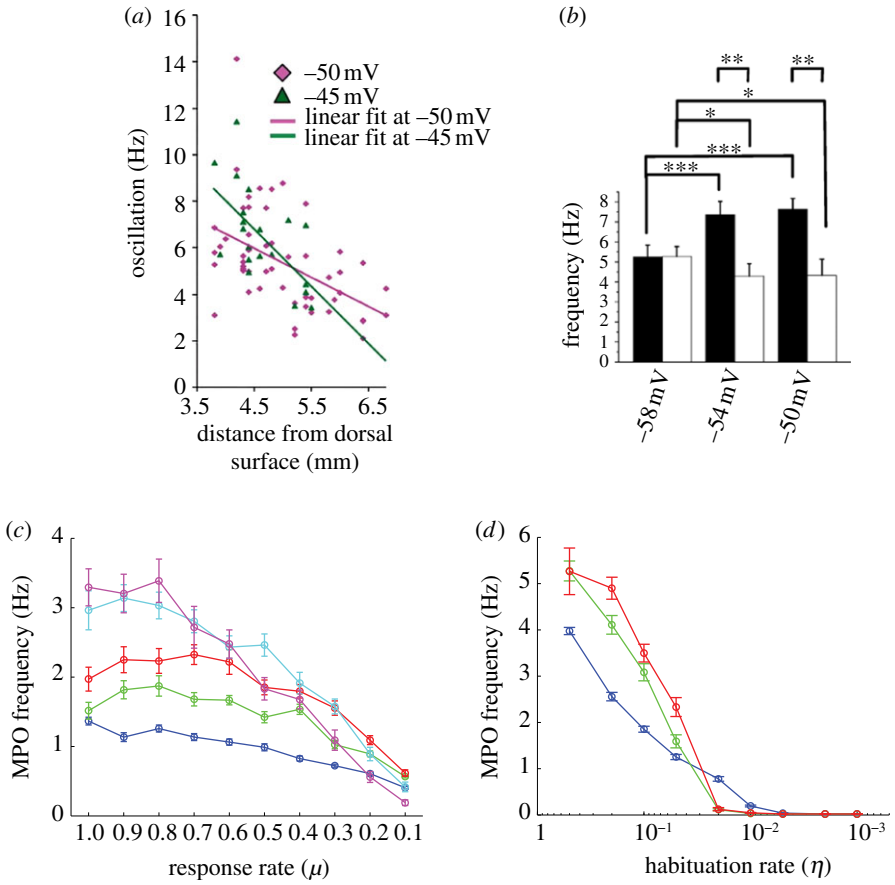

Figure 5. Membrane potential oscillations (MPOs) of medial entorhinal cells. (*a*) Data showing the frequency of MPOs of rat MEC layer II stellate cells at different anatomical locations along the dorsoventral axis for two current amplitudes [41]. (*b*) Data showing the frequency of subthreshold MPOs in the dorsal (filled bars) and ventral (open bars) groups of MEC layer II stellate cells at three different mean membrane potentials [44]. (*c*) Simulations of the frequency of MPOs of model map cells as a function of cell response rate μ (see equation (A 5)), which is proposed to decrease along the dorsoventral axis, for current injections of different amplitudes ($I = 0.5$ (blue); 1 (green); 1.5 (red); 2 (cyan); and 2.5 (magenta)). (*d*) Simulations of the frequency of MPOs of model map cells as a function of cell habituation rate η (see equation (A 7)) for current injections of different amplitudes ($I = 0.5$ (blue); 1 (green); 1.5 (red)). Error bars in (*b–d*) indicate SEM. Data repoduced with permission from [41] and [44]. Simulations reproduced with permission from [21].

sequential moments, and the overlap among firing periods from even these small ensembles of time cells bridges the entire delay. Notably, the spread of the firing period for each neuron increased with the peak firing time . . .'

It remains to be shown whether the spectrum of time cells arises from a gradient in a single-rate parameter, as is predicted by the spectral timing model. A biophysical interpretation of this rate parameter has been given in terms of calcium dynamics in the metabotropic glutamate receptor system for the case of spectral timing in the cerebellum [56]. The most parsimonious prediction is that a similar mechanism holds in all cases of spectral timing throughout the brain. To the present, spectral timing has been modelled in the HC, cerebellum and basal ganglia [57].

In summary, dorsoventral gradients in single-rate parameters within the entorhinal–hippocampal system may create multiple smaller spatial and temporal scales in the entorhinal cortices that can be fused into larger spatial and temporal scales in the hippocampal cortex, indeed scales that are large enough to control adaptive behaviours. The mechanistic homology between these spatial and temporal mechanisms suggests why they may occur side-by-side in the medial and lateral streams through entorhinal cortex into the HC. Spatial representations in the *Where* cortical stream go through postrhinal cortex and MEC on their way to hippocampal cortex, and object representations in the *What* cortical stream go through perirhinal cortex and LEC on their way to hippocampal cortex [58–62], where they are merged. This unity of mechanistically homologous space and time representations may be summarized by the term 'neural relativity'. The existence of computationally homologous spatial and temporal representations in the HC may help us to clarify its role in mediating episodic learning and memory, which has been studied since Tulving ([63]; see also [64]) proposed that each episode in memory consists of a specific spatio-temporal combination of stimuli and behaviour.

8. Homologous processing of angular and linear velocity path integration inputs

The inputs that drive the initial development of grid cells are vestibular angular and linear velocity signals that are activated by an animal's navigational movements. The model proposes that both angular and linear velocity signals are processed by ring attractor neural circuits. Angular velocity signals are integrated by head direction (HD) cells [65,66] that are often modelled as part of ring attractor circuits [67–74]. The position of an activity bump in a HD ring attractor maximally activates cells that code the current HD. Similarly, linear velocity signals are proposed to be integrated by ring attractors that are composed of stripe cells (see §3; figure 2; and equations

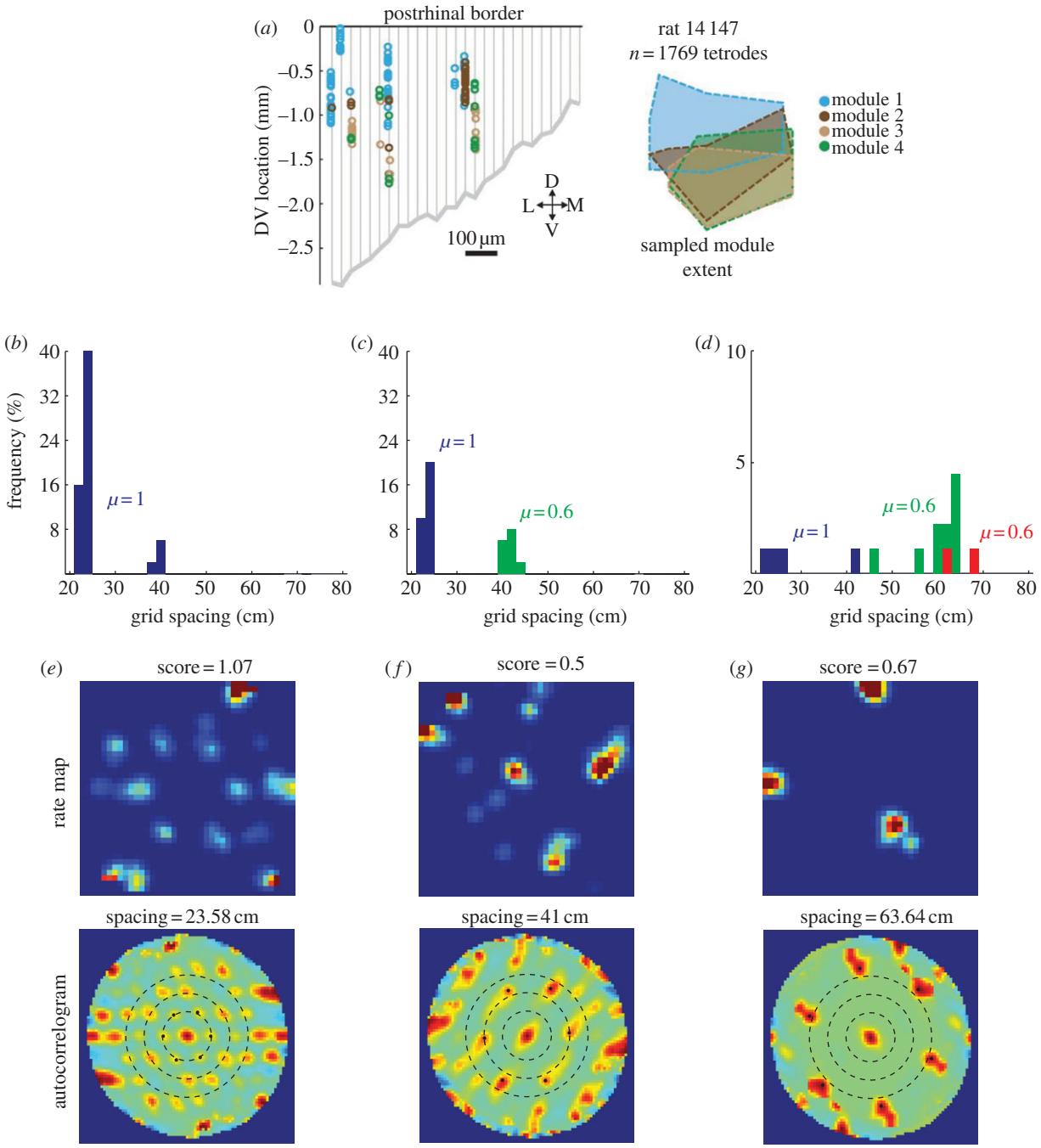

Figure 6. Anatomically overlapping grid cell modules. (*a*) Anatomical distribution of sampled grid cells belonging to different modules in one animal [15]. (*b–d*) Simulation results of the SOM model [21]. (*b*) Distribution of learned grid spacings in a SOM comprising 50 map cells, all with response rate (see equation (A 5)) $\mu = 1$, that are receiving adaptive inputs from stripe cells of two spacings ($s_1 = 20$ cm, $s_2 = 35$ cm). Only cells with gridness score > 0.3 are considered. (*c*) Distribution of learned grid spacings in a SOM comprising 50 cells, half with $\mu = 1$ and the remaining with $\mu = 0.6$, that are receiving adaptive inputs from stripe cells of two spacings ($s_1 = 20$ cm, $s_2 = 35$ cm). (*d*) Distribution of learned grid spacings in a SOM comprising 90 cells, one-third with $\mu = 1$, one-third with $\mu = 1$, and the remaining with $\mu = 0.3$, that are receiving adaptive inputs from stripe cells of three spacings ($s_1 = 20$, $s_2 = 35$, $s_3 = 50$ cm). (*e–g*) Spatial rate maps and autocorrelograms of illustrative grid cells with different learned spacings from the simulation summarized in (*d*). Peak activity A_s of stripe cells was 1, 0.8, 0.6 for spacings of 20, 35, 50 cm, respectively (see equation (A 4)). Colour coding from blue (min.) to red (max.) is used for each rate map, and from blue (−1) to red (1) for each autocorrelogram in (*e–g*). Data in (*a*) reproduced with permission from [15].

(A 1)–(A 4)). The outputs of HD cells modulate the linear velocity signals to create multiple directionally selective stripe cell ring attractor circuits, assuming heading direction is always tangential to the trajectory. This modulation is sensitive to the cosine of the difference between the current heading direction of movement and the ring attractor's directional preference. As noted in §3, each stripe cell ring attractor is also selective to a different spatial scale. Stripe cells within each such ring attractor circuit are activated at different spatial phases as an activity bump moves across their ring locations. They code displacement in a given direction, and may be activated periodically as the activity bump moves around the ring more than once in response to the animal's navigational movements.

The model's assumption that both HD cells and stripe cells are computed by ring attractors that drive grid and place cell development is consistent with data showing that adult-like HD cells exist in parahippocampal regions of rat pups when they actively move out of their nests for the first time at around two weeks of age [30,31]. The predicted existence of stripe cells has received some experimental

support from a report of cells with similar spatial firing properties in dorsal parasubiculum [75], which projects directly to layer II of MEC [76,77].

Blair *et al*. [78] also discuss ring attractors for linear velocity path integration. In their conception, however, this 'is produced by subcortical ring attractor networks that function as frequency-modulated oscillators, and that these networks provide the neural substrate for storing and updating the phase-coded position signal . . . In accordance with the principles of oscillatory interference, we show that outputs from theta cells residing in different (but not the same) ring attractors can be combined to form spatially periodic oscillations, which are similar to the observed firing patterns of grid cells'. By contrast, the stripe cell ring attractor is phasically driven by linear velocity signals created by movements through an environment. Ring attractors for representing HD also do not endogenously oscillate. They are also phasically driven by angular velocity signals when the head moves, hence their close mechanistic homology to the stripe cell ring attractor in the SOM model.

9. Stable learning, attention, realignment and remapping

Place cell selectivity can develop within seconds to minutes, and can remain stable for months [70–82]. The HC needs additional mechanisms to ensure this long-term stability. This combination of fast learning and stable memory is often called the *stability–plasticity dilemma* [83,84]. SOMs are themselves insufficient to solve the stability–plasticity dilemma in environments whose input patterns are dense and are non-stationary through time [26,85], as occurs regularly during real-world navigation.

Adaptive resonance theory (ART) proposes how to dynamically stabilize the learned categorical memories of SOMs. ART is a cognitive and neural theory of how the brain autonomously learns to attend, recognize and predict objects and events in a changing world. ART shows how SOMs may be augmented by learned top-down expectations that are matched against bottom-up signals by an ART matching rule. ART proposes that top-down expectations focus attention on salient combinations of features, while suppressing unmatched features. ART hereby explains how such top-down attentive matching may help to solve the stability–plasticity dilemma. In particular, when a good enough match occurs, a synchronous resonant state emerges that embodies an attentional focus and is capable of driving fast learning by the adaptive weights that control activation of bottom-up recognition categories and top-down expectations; hence the name *adaptive* resonance.

Specific anatomical and neurophysiological properties of this top-down ART matching rule have been predicted and subsequently supported by experiments on many kinds of psychological and neurobiological data (see [84] and [86] for reviews). In particular, the ART matching rule predicts that attention is realized by a top-down, modulatory on-centre, driving off-surround network, which predicts and computationally instantiates the heuristic concept of attention as 'biased competition' [87].

Experimental data about the HC from several laboratories are compatible with ART predictions about the role of top-down expectations and attentional matching in memory stabilization. Kentros *et al*. [88] reported that 'conditions that maximize place field stability greatly increase orientation to novel cues. This suggests that storage and retrieval of place cells is modulated by a top-down cognitive process resembling attention and that place cells are neural correlates of spatial memory', and that NMDA receptors mediate long-lasting hippocampal place field memory in novel environments [89]. Morris & Frey [90] proposed that hippocampal plasticity reflects an 'automatic recording of attended experience'. Bonnevie *et al*. [91] showed that hippocampal inactivation causes grid cells to lose their spatial firing patterns; see §12 for an explanation and simulation of these data that is compatible with the ART matching rule. These experiments clarify how cognitive processes such as attention may play a role in entorhinal–hippocampal spatial learning and memory stability. The proposed mechanism of top-down attentional matching may also help to clarify data about grid realignment and place remapping, and tight distributions of grid orientations for similar grid scales.

10. Beta and gamma oscillations

Within ART, a sufficiently good top-down match with bottom-up signal patterns can trigger fast gamma oscillations that enable spike-timing-dependent plasticity to occur, whereas a big enough mismatch can trigger slow beta oscillations and a shift of attention, while inhibiting learning [92]. Beta oscillations have been reported in the HC during the learning of place fields in novel environments [93], and have the properties expected when mismatches occur and receptive field refinements are learned [94]. Berke *et al*. [93] showed that, paradoxically, beta power was very low as a mouse traversed a lap for the first time in a novel environment, grew to full strength on the second and third laps, became low again after 2 min of exploration, and remained low on subsequent days. Beta oscillation power also correlated with the rate at which place cells became spatially selective, but not with theta oscillations. These data can be explained as follows [94]: in any ART system, the top-down adaptive weights that represent learned expectations need to all be sufficiently large before learning occurs, so that they can match whatever input pattern first initiates learning of a new category [85]. Indeed, when a new category is first activated, it is not known at the category level what pattern of features caused the category to be activated. Whatever feature pattern was active needs to be matched by the top-down expectation on the first learning trial, so that resonance and weight learning can occur; hence, the need for the initial values of all top-down weights to be sufficiently large to match any input pattern. The low beta power on the first lap of exploration can be explained by the initial top-down match.

Given that top-down weights are initially broadly distributed, the learning of top-down expectations is a process of pruning weights on subsequent trials, and uses mismatch-based reset events to discover categories capable of best representing the environment. Beta power on subsequent laps can be explained by mismatch reset events that correlate with the rate at which place cells become spatially selective. After learning stabilizes, there are no more mismatches, so beta power subsides. Such an inverted-U in beta power through time is thus a signature of ART category learning in any environment.

Recent neurophysiological data suggest that beta oscillations also occur as predicted in the deeper layers of the

visual cortex [95], and in the frontal eye fields and extrastriate cortical area V4 during shifts in spatial attention [96]. Thus, the match/mismatch dynamics leading to gamma/beta oscillations seem to occur in multiple brain systems.

11. Effects on grid cells of inactivating medial septum and the theta rhythm

The theta rhythm has been associated with properties of spatial navigation. The medial septum (MS) in the basal forebrain plays an important role in generating and maintaining network theta rhythm in the hippocampal and parahippocampal areas [97] via reciprocal interactions among GABAergic interneurons [98,99]. Recent experiments have reduced the theta rhythm by inactivating the MS and demonstrated a correlated reduction in the hexagonal spatial firing patterns of grid cells [100,101] (figure 7*a*,*b*). These results, along with properties of intrinsic MPOs in slice preparations of entorhinal cells [41], have been interpreted to support oscillatory interference accounts of grid cells. However, the SOM model of grid cell learning can explain these data without invoking oscillatory interference [24].

In particular, the adverse effects of MS inactivation on grid cells are related in the model to how the concomitant reduction in cholinergic inputs may increase conductances of leak potassium and slow and medium after-hyperpolarization channels (figure 7*c*–*e*), which, in turn, cause delayed and reduced excitability with longer refractory periods. Model simulations show spatial disorganization of grid fields in addition to reductions in firing rate and spatial stability, when MS inactivation is invoked by either a temporary reduction in cell response rates μ (see equation (A 5)) from 1 to 0.25 (figure 7*c*,*d*), or a temporary increase in leak conductances A (see equation (A 5)) from 3 to 3.5 combined with a temporary decrease in habituation rates η (see equation (A 7)) from 0.05 to 0.0125 (figure 7*e*).

Koenig *et al*. [101] also examined the effects of inactivating MS on hippocampal place cells, and found that they largely maintain their place fields, but show reductions in firing rate and theta band modulation. This provides additional support to our SOM model's prediction that the theta rhythm is not crucial for medial entorhinal–hippocampal cells to encode spatial information. Longer refractory periods that result from reduced cholinergic action do not adversely affect place cells because they do not have the multiple periodic spatial fields of grid cells and, in addition to grid cell inputs, they also receive reliable sensory, notably visual, inputs in a familiar environment.

12. Three types of grid cell models: effects on grid cells of inactivating hippocampus

Models of grid cells can be divided into three classes: SOM [17,22,23], continuous attractor [12,102–104] and oscillatory interference models [35,36,105]. Zilli [106] reviews some basic properties of these models. This section briefly summarizes some of the problematic properties of continuous attractor and oscillatory interference models that we believe may be overcome by SOM models. One issue that remains to be resolved is that only SOM models have demonstrated how grid cell receptive fields may arise through self-organized real-time learning with local interaction laws as an animal navigates realistic trajectories. Kropff & Treves [107] provide the only other type of grid cell learning model, which is, however, not based on path integration, but on adaptive inputs from place cells. This developmental hypothesis is arguable as grid cells show spatial responses in any environment, unlike place cells [108]. In addition, Kropff & Treves [107] use an algorithmic iterative normalization of cell activities and adaptive weights—hence it is not a real-time model—and simulates far less data than the SOM model. As no single model has yet explained all available data about grid cells and place cells, further development of all these models, and possible hybrids thereof, may be expected.

Oscillatory interference models propose that the grid pattern arises due to interference among a baseline oscillation of fixed frequency and multiple oscillations whose frequencies are modulated by components of linear velocity along their particular preferred allocentric directions. As noted in §5, the mean frequencies of subthreshold MPOs in MEC layer II stellate cells decrease with their positions along the dorsoventral axis, and thus inversely correlate with the spatial scales of the grids [41]. Again, these data properties are not compelling evidence for oscillatory interference because they have also been simulated using the self-organized grid cells of the SOM model [21].

To generate a hexagonal grid pattern, the interference models require the selective combination of three directional band cell oscillators whose preferred directions are 60° apart from each other. Any other combination leads to dramatically different firing fields that have not been observed [36]. On the other hand, as mentioned in §§3, 5 and 6, the SOM model can self-organize hexagonal grids as well as their anatomical and neurophysiological properties along the dorsoventral axis in response to stripe cells of multiple directions, phases and scales [21].

The interfering oscillations are assumed to have frequencies in the theta band (4–11 Hz). If grid cells can exist without theta oscillations, then the foundational hypothesis of oscillatory interference models would not be supported. Indeed, Yartsev *et al.* [109] have shown that hexagonal grid firing fields in crawling bats can occur in the absence of theta band modulation. Moreover, [110] and [111] used *in vivo* whole-cell recordings during virtual reality navigation to conclude that the spatial field-selective firing of grid cells is better explained by membrane potential ramps caused by integration of synaptic inputs on a slower, subtheta timescale, and not by constructive interference among intrinsic MPOs in the theta band.

Despite these differences, oscillatory interference and SOM models share a basic design constraint that contrasts with continuous attractor models: they both assume that two-dimensional hexagonal grids arise from input combinations of one-dimensional band cells or stripe cells, respectively.

Continuous attractor models propose that grid cell firing may arise directly from recurrent interactions in a two-dimensional network of grid cells in response to path integration inputs. One problem with these models is that their network connections are finely tuned and have spatially anisotropic weights, notably asymmetric two-dimensional recurrent inhibitory interactions. These asymmetric connection weights may be difficult to justify biologically without either experimental evidence that they exist, or at least simulations showing how this weight structure can be learned during navigation. This is especially challenging given that anatomically nearby grid cells can belong to different scale-specific modules [15], which raises the issue of how such cells may be

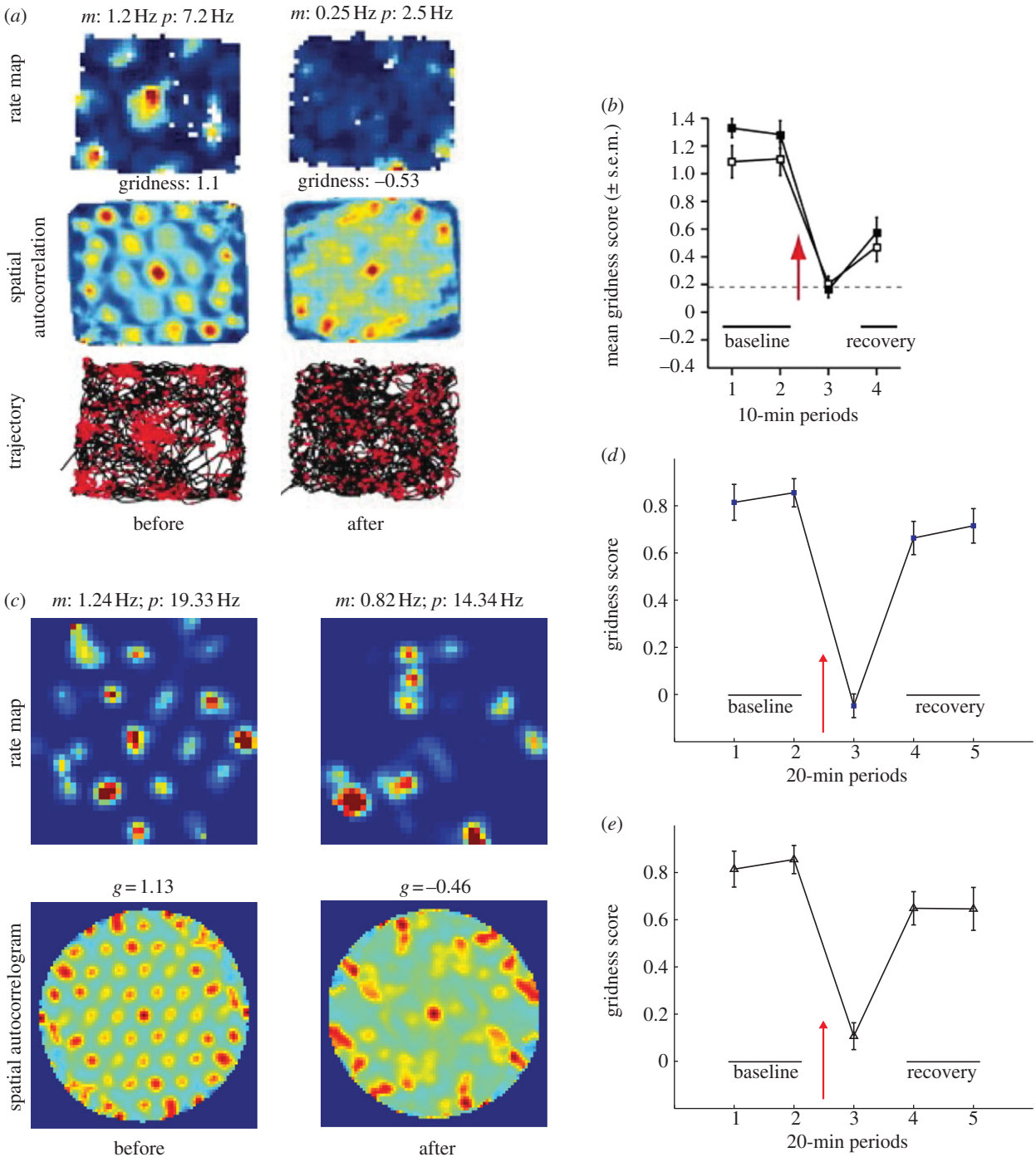

Figure 7. Effects of medial septum (MS) inactivation on grid cells. (*a*) Data showing the adverse effect on the hexagonal grid spatial responses of a grid cell when MS in inactivated [100]; compare left subpanels with right ones. (*b*) Data summarizing the temporary reduction in gridness score of grid cells during MS inactivation [101]. (*c*) Spatial responses of a learned model grid cell before and after MS in inactivated [24]. The cell was from an entorhinal SOM receiving adaptive inputs from stripe cells of two spacings ($s_1 = 20$ cm, $s_2 = 35$ cm). MS inactivation was invoked by a reduction in cell response rates μ (see equation (A 5)) from 1 to 0.25, mimicking reduced cholinergic transmission. (*d*) Simulations of temporary reduction in gridness score of model grid cells as a result of abrupt changes in cell response rates μ from 1 to 0.25 for one trial [24]. (*e*) Simulations of temporary reduction in gridness score of model grid cells as a result of abrupt changes in leak conductances A (see equation (A 5)) and habituation rates η (see equation (A 7)) from 3 to 3.5 and from 0.05 to 0.0125, respectively, for one trial. Results in (*d*,*e*) are for model grid cells with a gridness score >0 in the trial immediately preceding the one coinciding with the inactivated MS. The red arrow in (*b*,*d*,*e*) signifies MS inactivation. Colour coding from blue (min.) to red (max.) is used for each rate map, and from blue (-1) to red (1) for each autocorrelogram in (*a*,*b*). Data in (*a*,*c*) reproduced with permission from [100] and [101], respectively. Simulations adapted with permission from [24].

developmentally segregated into different attractor networks, and given that spatial fields of grid cells that share the same scale do not exhibit any notable topographic organization [11].

By contrast, the SOM model can develop grid and place cells using spatially isotropic recurrent inhibitory connections. The SOM model has directional asymmetries in the various one-dimensional stripe cell ring attractors for path integration, rather than directly in a two-dimensional field of grid cells. It is legitimate to ask why such connections in a one-dimensional ring attractor may be more plausible than directionally asymmetric connections across a two-dimensional attractor network. The proposed homology in the design of stripe cell and HD cell ring attractors (§8) provides some evidence for this. More generally, whatever mechanism turns out be used

by HD cells can be co-opted for stripe cells. The existence of stripe-like cells in parasubiculum also provides some experimental evidence [75].

In addition, it is easy to imagine how a developmental gradient among the cells in a one-dimensional network like a ring attractor can cause the strengths of inhibitory connections to be greater in one direction than the opposite direction. It is harder to imagine how directionally specific two-dimensional inhibitory receptive fields can be learned and superimposed in space, as required in a continuous attractor model.

In the one-dimensional case, asymmetric inhibitory interactions in a HD cell ring attractor suffice to move an activity bump across the network's HD cells in response to angular velocity inputs. Given such an asymmetric gradient, the key problem is how the HD cells can be calibrated to represent prescribed HDs. The HeadMoVVes model [74] has simulated how path integration motor inflow inputs, motor outflow movement commands, and visual feedback to a ring attractor of HD cells may be calibrated by learning. The resultant learned cell properties simulate data about the neurophysiology of HD cells in the multiple brain regions that are used by the brain to calibrate HD. This model hereby provides a proof of principle that learned calibration of one-dimensional ring attractors is possible.

The continuous attractor model of [38] and [91] proposes how hexagonal grid cell responses may arise as a result of interactions among a bottom-up directionally modulated velocity input, a spatially uniform excitatory top-down input from the HC, and recurrent inhibition governed by two-dimensional spatially anisotropic connectivity. This model has been used to explain effects on grid cell firing of focal hippocampal inactivation [91], notably an extinction of the grid pattern owing to dispersion in spike locations, a drop in the average firing rate and an emergence of grid cell tuning to HD (though weak and unstable; figure 8*a*). When the uniform excitatory input is shut off, similar properties occur in the model [91].

Both the excitatory and inhibitory interactions that are posited in their model raise questions. The model assumes that the two-dimensional asymmetric recurrent inhibitory connections of each cell are sensitive to its preferred direction. As noted above, there seems currently to be no experimental evidence to support this assumption. It is also not clear how the dependence on a single directional preference in both bottom-up and recurrent interaction kernels would develop. The assumption that the top-down input to grid cells from the HC is a spatially uniform and driving input seems to be incompatible with the most basic properties of place cell firing that are selective to specific places of an environment (§1), and with data from several laboratories which suggest that top-down attentional connections underlie dynamic stabilization of hippocampal spatial memory (§9) [88–90,93,112]. Such an attentional matching input would be expected to be spatially selective, not uniform. It would also not be driving excitatory input, because attention is known to have a modulatory on-centre in all other modalities where it has been studied.

Can hippocampal inactivation cause the observed grid cell changes if the top-down hippocampal input instantiates a form of attentional modulation that dynamically stabilizes learned grid cell properties (§9)? At least two types of effects might be expected theoretically: first, disorganization of the grid pattern when the stabilizing top-down input is removed. Second, reduction in the resultant disorganized grid cell firing levels owing to a larger influence of inhibitory inputs caused by removal of the top-down input. Figure 8*b*,*c* summarizes simulations that use noise-free and noisy path integration inputs, respectively, to illustrate how destabilization of grid fields could occur when top-down attention is removed. The noisy case also includes an extra uniform inhibitory signal to illustrate the increased inhibitory effects of removing top-down attention in the simplest possible way. Top-down attention typically has a modulatory on-centre, but it also causes driving inhibition in its off-surround (§9). If only some hippocampal cells (e.g. dorsal) were silenced, then this could disinhibit nearby hippocampal cells, thereby possibly strengthening their driving inhibitory off-surround inputs to the grid cells that lost their excitatory hippocampal modulation. In addition, attentionally modulated grid cells could inhibit their unmodulated neighbours more than conversely. The net effect could be to significantly increase the inhibition of the unmodulated grid cells. This effect was, thus, approximated by delivering an extra uniform inhibitory signal to the affected grid cells. Dynamic (spike-triggered) autocorrelograms based on a time window of 10 s reveal the lack of a grid pattern in the noisy case (figure 8*b*,*c*). This suggests that uncorrected positional drift through the trial as a consequence of hippocampal inactivation is indeed capable of diminishing the expression of grid structure. The SOM equations and parameters that were used in the inactivation simulations are provided in appendix B.

Another relevant factor in the firing of grid cells is the ability of cells in a normal SOM network to respond more strongly to the most frequent and energetic combinations of inputs. If upsetting the excitatory–inhibitory balance could shift the response threshold to lower values, then the effects of individual stripe cells might be more evident in grid cell responses. These, in turn, may help to explain the head directional influence on grid cell firing after hippocampal inactivation. These effects in the current simulations can occur more quickly than in the data. A more realistic time course could be simulated by matching the rate with which inactivation occurs in the HC, as in the data.

These types of factors are worthy of further experimental and theoretical study. Experiments to further test the existence and predicted properties of bottom-up stripe cells and of top-down attentional matching signals would be particularly informative towards settling these issues.

Funding statement. This work was supported in part by the SyNAPSE programme of DARPA (HR0011-09-C-0001).

Appendix A. Grid cell module simulations

This section describes the rate-based spectral spacing model equations [21] that were used in simulations of grid cell modules [15] shown in figure 6.

A.1. Stripe cells

Stripe cells are algorithmically computed, for the sake of simplicity, as follows: if at time t the animal heads along allocentric direction $\varphi(t)$ with velocity $v(t)$, then the velocity $v_d(t)$ along direction d is

$$v_d(t) = \cos(d - \varphi(t))v(t). \quad (A\,1)$$

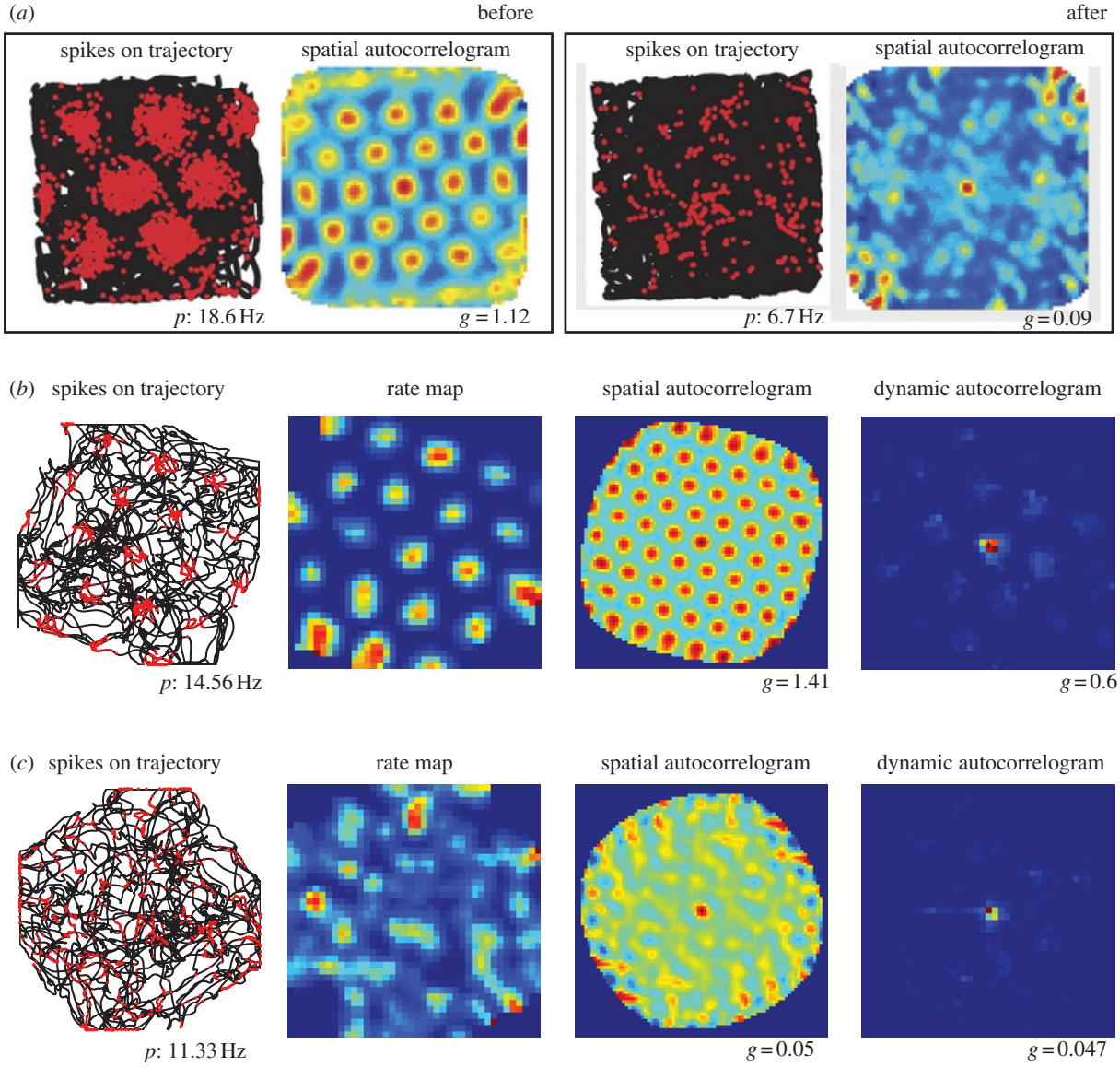

Figure 8. Role of hippocampal feedback in maintaining grid fields. (*a*) Data showing the effect of hippocampal inactivation on a grid cell [91]. (*b*) Spatial responses of a learned spiking model grid cell in response to noise-free path integration inputs [25], approximating the baseline condition in which hippocampal place cells provide stabilizing top-down inputs to grid cells that are suggested to regularly correct path integration errors in a familiar environment. The four subpanels from left to right show the map of spike locations (red dots) superimposed on the trajectory of the animal (black line) through time, the smoothed spatial rate map, the spatial autocorrelogram (200 × 200 cm) and the dynamic (spike-triggered) autocorrelogram (100 × 100 cm), respectively. The dynamic autocorrelogram is based on a time window of 10 s. (*c*) Spatial responses of the same cell during simulated hippocampal inactivation in response to noisy path integration with an extra non-specific tonic inhibitory input of 5 Hz (A_{off}). The ground truth linear velocity values were additively corrupted by Brownian motion with a standard deviation σ_{noise} of 3 cm. See appendix B for details. Consistent with data [91], there is not only a reduction in the gridness score (note values (*g*) below subpanels showing spatial autocorrelograms), but also a drop in the peak firing rates (note values (*p*) below subpanels showing spikes on trajectories). Gridness scores for dynamic autocorrelograms were computed using the method described in [30]. Colour coding from blue (min.) to red (max.) is used for each rate map, from blue (−1) to red (1) for each spatial autocorrelogram, and from blue (0) to red (1) for each dynamic autocorrelogram. Data in (*a*) reproduced with permission from [91].

The displacement $D_d(t)$ traversed along direction d with respect to the initial position is calculated by path integration of the corresponding velocity:

$$D_d(t) = \int_0^t v_d(\tau)\mathrm{d}\tau. \tag{A 2}$$

This directional displacement variable is converted into activations of various stripe cells. Let $S_{dps}(t)$ be the activity of a stripe cell whose spatial fields are oriented perpendicular to direction d with spatial phase p and spatial period s. It will be maximal at periodic positions $ns + p$ along direction d, for all integer values of n. In other words, $S_{dps}(t)$ will be maximal whenever (D_d modulo s) $= p$. Defining the spatial phase difference ω_{dps} between D_d and p with respect to spatial scale s by:

$$\omega_{dps}(t) = (D_d(t) - p) \quad \text{modulo} \quad s, \tag{A 3}$$

the stripe cell activity $S_{dps}(t)$ is modelled by a Gaussian tuning function:

$$S_{dps}(t) = A_s \cdot \exp\left(-\frac{(\min(\omega_{dps}(t), s - \omega_{dps}(t)))^2}{2\sigma_s^2}\right), \tag{A 4}$$

where A_s is the maximal activity and σ_s is the standard deviation of each of its individual stripe fields along preferred

direction d. All directional displacement variables $D_d(t)$ were initialized to 0 at the start of each learning trial.

A.2. Map cells

The membrane potential V_j^m of the MEC layer II map cell j in local population m obeys membrane equation, or shunting, dynamics within a recurrent on-centre off-surround network [26,83] as follows

$$\frac{dV_j^m}{dt} = 10\mu_j\left[-AV_j^m + (B - V_j^m)\left(\sum_{dps} w_{dpsj}^m x_{dps} + \alpha([V_j^m]^+)^2 z_j^m\right) - (C + V_j^m)\sum_{k\neq j}\beta([V_k^m - \Gamma]^+)^2\right], \quad \text{(A 5)}$$

where μ_j controls the rate of temporal integration of the cell (called the response rate); A is the decay parameter corresponding to the leak conductance; B and $-C$ are the reversal potentials of the excitatory and inhibitory channels, respectively; w_{dpsj}^m is the synaptic weight of the projection from the stripe cell with activity S_{dps} in equation (A 4) to the map cell j in population m; $\alpha([V_j^m]^+)^2$ is the on-centre self-excitatory feedback signal of the cell, which helps to resolve the competition among map cells within cell population m, where $[V]^+ = \max(V,0)$ defines a threshold-linear function, and α is the gain coefficient; z_j^m is the habituative transmitter gate of map cell j; and β is the connection strength of the inhibitory signal $([V_k^m - \Gamma]^+)^2$ from map cell k in the off-surround to map cell j within population m. The output activity of map cell j is given by $([V_j^m - \Gamma]^+)^2$, which is the same as its recurrent inhibitory signal to other cells in the population. The membrane potential of each map cell was initialized to 0 at the start of each trial.

A.3. Adaptive weights

The adaptive weights w_{dpsj}^m of projections from stripe cells to map cells are governed by a variant of the competitive instar learning law [26,34]:

$$\frac{dw_{dpsj}^m}{dt} = \lambda([V_j^m - \Gamma]^+)^2 \times \left[(1 - w_{dpsj}^m)x_{dps} - w_{dpsj}^m \sum_{(p,q,r)\neq(d,p,s)} x_{pqr}\right], \quad \text{(A 6)}$$

where λ is the learning rate; the map cell output signal $([V_j^m - \Gamma]^+)^2$ gates learning on and off; and the learning rule defines a self-normalizing competition among afferent synaptic weights to the target cell, leading to a maximum learned total weight to the cell of 1. Each weight w_{dpsj}^m was initialized to a random value drawn from a uniform distribution between 0 and 0.1 at the start of the first trial.

A.4. Habituative gating

The habituative transmitter z_j^m of map cell j in population m is defined by

$$\frac{dz_j^m}{dt} = 10\eta[(1 - z_j^m) - \gamma z_j^m(\alpha([V_j^m]^+)^2)^2], \quad \text{(A 7)}$$

where η controls the overall response rate of the transmitter (called the habituation rate) and γ modulates its depletion rate. In particular, term $(1 - z_j^m)$ controls the gate recovery rate to the target level of 1, and term $-\gamma z_j^m(\alpha([V_j^m]^+)^2)^2$ controls the gate inactivation rate, which is proportional to the current gate strength z_j^m times the square of the signal $(\alpha([V_j^m]^+)^2)$ that z_j^m gates in equation (A 5). The squaring operation causes the gated signal to first increase and then decrease through time in response to excitatory input (cf. [113]), thereby regulating the duration of intense cell activity, and thus cell perseveration. The habituative transmitter of each map cell was initialized to its maximum value of 1 at the start of each trial.

A.5. Simulation settings

The parameter values used in the simulations were $A = 3$; $B = 1$; $C = 0.5$; $\alpha = 17.5$; $\beta = 1.5$; $\gamma = 0.2$; $\lambda = 0.025$; $\eta = 0.05$ and $\Gamma = 0.1$. The differential equations governing model dynamics were numerically integrated using Euler's forward method with a fixed time step $\Delta t = 2$ ms.

We simulated the development of three entorhinal SOMs: one comprising 50 map cells, all with response rate $\mu = 1$, that received adaptive inputs from stripe cells of two spacings ($s_1 = 20$ cm, $s_2 = 35$ cm); one comprising 50 cells, half with $\mu = 1$ and the remaining with $\mu = 0.6$, that received adaptive inputs from stripe cells of two spacings ($s_1 = 20$ cm, $s_2 = 35$ cm); and the other comprising 90 cells, one-third with $\mu = 1$, one-third with $\mu = 1$, and the remaining with $\mu = 0.3$, that received adaptive inputs from stripe cells of three spacings ($s_1 = 20$ cm, $s_2 = 35$ cm, $s_3 = 50$ cm). In each case, stripe cells also varied with nine direction preferences (-80° to 80° in steps of 20°), and four spatial phases ($p = [0, s/4, s/2, 3s/4]$ for the stripe spacing s) per direction. Peak activity A_s of stripe cells were set to 1, 0.8, 0.6 for spacings of 20, 35, 50 cm, respectively. The standard deviation σ_s of each stripe field Gaussian tuning was set to 8.84% of the stripe spacing. The development of the entorhinal map cells into their adult counterparts was accomplished by using 20 trials, in each of which the animal ran along a novel realistic trajectory of approximately 20 min in a circular environment with a radius of 50 cm. These trajectories were obtained by rotating an original rat trajectory (data: [13]) about the midpoint of the environment, which is also the starting point, by random angles. The original trajectory was, also, interpolated to increase its temporal resolution to match the time step of numerical integration of model dynamics ($\Delta t = 2$ ms).

A.6. Post-processing

The 100×100 cm environment was divided into 2.5×2.5 cm bins. During each trial, the amount of time spent by the animal in the various bins was tracked. The output activity of each map cell in every spatial bin was accumulated as the trajectory visited that bin. The occupancy and activity maps were smoothed using a 5×5 Gaussian kernel with standard deviation equal to unity. At the end of each trial, smoothed rate maps for each map cell were obtained by dividing the cumulative activity variable by cumulative occupancy variable in each bin. For each map cell, six local maxima with $r > 0.05$ and closest to the central peak in the spatial autocorrelogram of its smoothed rate map were identified. Gridness score, which measures how hexagonal and

periodic a grid pattern is, was then derived using the method described in [31], and grid spacing was obtained as the median of the distances of the six local maxima from the central peak [11].

Appendix B. Hippocampal inactivation simulations

This section describes the spiking GridPlaceMap model equations [25] that were used in simulations of the effects on grid cells of hippocampal inactivation [91] shown in figure 8.

B.1. Stripe cells

See appendix A for basic details of stripe cells. Given the spiking implementation, non-homogeneous Poisson spike trains are generated for the various stripe cells S_{dps} using the method of infinitesimal increments. Briefly, a cell with an instantaneous firing rate of λ fires a spike within an infinitesimal duration (Δt) if $p(\text{spike}) = e^{-\lambda\Delta t}(\lambda\Delta t)^1/1! \approx \lambda\Delta t$ is greater than a random number sampled from a uniform distribution between 0 and 1.

B.2. Map cells

The membrane potential V^g_{js} of the jth MEC map cell of scale s is defined by a membrane equation that obeys shunting integrate-and-fire dynamics within a recurrent competitive network:

$$C_m \frac{dV^g_{js}}{dt} = g_{\text{LEAK}}(E_{\text{LEAK}} - V^g_{js}) + \sum_{dp} g_{\text{NMDA}} B(V^g_{js}) x^s_{dps} w^g_{dpsj} (E_{\text{NMDA}} - V^g_{js}) + g_{\text{GABA}}(E_{\text{GABA}} - V^g_{js}) \left(\sum_{J \neq j} x^g_{Js} + x_{\text{off}} \right), \quad \text{(B 1)}$$

where C_m is membrane capacitance; g_{LEAK} is the constant conductance of the leak Cl^- channel; E_{LEAK} is the reversal potential of the leak Cl^- channel; g_{NMDA} is the maximal conductance of each excitatory NMDA receptor-mediated channel; E_{NMDA} is the corresponding reversal potential; g_{GABA} is the maximal conductance of each inhibitory, $GABA_A$ receptor-mediated channel; E_{GABA} is the corresponding reversal potential; $B(V) = 3.708/1 + e^{-0.0174V}$ defines the voltage-dependent removal of the Mg^{2+} block in the NMDA channel; x^s_{dps} is the NMDA channel gating variable that is controlled by the spiking of the stripe cell that codes direction d, phase p and scale s; w^g_{dpsj} is the synaptic weight of the projection from this stripe cell to the jth MEC map cell of scale s; x^g_{Js} is the $GABA_A$ channel conductance gate that is opened by the spiking of the Jth MEC map cell of scale s in the off-surround; and x_{off} is the $GABA_A$ channel conductance gate that is opened by a non-specific tonic inhibitory input when HC is inactivated. The dynamics of the NMDA channel gating variable x^s_{dps} obey a mass action law:

$$\frac{dx^s_{dps}}{dt} = -\frac{x^s_{dps}}{\tau^{\text{NMDA}}_{\text{decay}}} + \alpha(1 - x^s_{dps}) a^s_{dps}, \quad \text{(B 2)}$$

where the secondary gating variable a^s_{dps} obeys

$$\frac{da^s_{dps}}{dt} = -\frac{a^s_{dps}}{\tau^{\text{NMDA}}_{\text{rise}}}, \quad \text{and} \quad a^s_{dps} \to 1 \quad \text{(B 3)}$$

whenever the stripe cell that codes direction d, phase p, and scale s spikes.

Whenever the membrane potential V^g_{js} reaches the spiking threshold V_{th}, it is reset to V_{reset}, and the map cell triggers an output spike. The dynamics of the $GABA_A$ channel conductance gate x^g_{Js} obey

$$\frac{dx^g_{Js}}{dt} = -\frac{x^g_{Js}}{\tau^{\text{GABA}}}, \quad \text{and} \quad x^g_{Js} \to 1 \quad \text{(B 4)}$$

whenever the J^{th} MEC map cells of scale s spikes, and the dynamics of the $GABA_A$ channel conductance gate x_{off} obey

$$\frac{dx_{\text{off}}}{dt} = -\frac{x_{\text{off}}}{\tau^{\text{GABA}}}, \quad \text{and} \quad x_{\text{off}} \to 1 \quad \text{(B 5)}$$

at a tonic frequency of A_{off} during hippocampal inactivation.

All gates are initialized to zero, and all membrane potentials are initialized to V_{rest} at the start of each trial.

B.3. Adaptive weights

The adaptive weights, w^g_{dpsj}, of the synaptic connections from stripe cells to MEC cells are modified using a spike-timing-dependent variant of the competitive instar learning law, as follows:

$$\frac{dw^g_{dpsj}}{dt} = \lambda_w y^g_{js} \left[y^s_{dps}(1 - w^g_{dpsj}) - w^g_{dpsj} \sum_{DP \neq dp} y^s_{DPs} \right], \quad \text{(B 6)}$$

where λ_w scales the rate of learning; y^g_{js} is a learning gate that is opened transiently by the spiking of the postsynaptic map cell V^g_{js}; and y^s_{dps} is an exponentially decaying trace variable that tracks the spiking activity of the stripe cell that codes direction d, phase p and scale s. The dynamics of the learning gate y^g_{js} and the trace variable y^s_{dps} obey

$$\frac{dy^g_{js}}{dt} = -\frac{y^g_{js}}{\tau}, \quad \text{and} \quad y^g_{js} \to 1 \quad \text{(B 7)}$$

whenever the jth MEC map cell of scale s spikes.

$$\frac{dy^s_{dps}}{dt} = -\frac{y^s_{dps}}{\tau}, \quad \text{and} \quad y^s_{dps} \to 1 \quad \text{(B 8)}$$

whenever the stripe cell that codes direction d, phase p, and and scale s spikes.

All gates are initialized to zero at the start of each trial. The weights are only initialized once, at the start of the first trial, by sampling from a uniform distribution between 0 and 0.1.

B.4. Simulation settings

The parameter values used in the simulations were $C_m = 1\ \mu\text{F cm}^{-2}$; $g_{\text{LEAK}} = 0.0005\ \text{mS cm}^{-2}$; $E_{\text{LEAK}} = -65\ \text{mV}$; $g_{\text{NMDA}} = 0.025\ \text{mS cm}^{-2}$; $E_{\text{NMDA}} = 0\ \text{mV}$; $g_{\text{GABA}} = 0.0125\ \text{mS cm}^{-2}$; $E_{\text{GABA}} = -70\ \text{mV}$; $\tau^{\text{NMDA}}_{\text{rise}} = 5\ \text{ms}$; $\tau^{\text{NMDA}}_{\text{decay}} = 50\ \text{ms}$; $\alpha = 1000$; $\tau^{\text{GABA}} = 10\ \text{ms}$; $\tau = 50\ \text{ms}$; $V_{\text{rest}} = -65\ \text{mV}$; $V_{\text{th}} = -50\ \text{mV}$; $V_{\text{reset}} = -60\ \text{mV}$; and $\lambda_w = 0.001$. The differential equations governing membrane potential and synaptic

weight dynamics were numerically integrated using Euler's forward method with a fixed time step $\Delta t = 2$ ms.

We first simulated the development of an entorhinal SOM, which included 100 map cells receiving adaptive inputs from 90 stripe cells with spacing $s_1 = 20$ cm, 18 direction preferences (d: -90° to 80° in steps of 10°), and five spatial phases ($p = [0, s/5, 2s/5, 3s/5, 4s/5]$ for the stripe spacing s) per direction. Peak firing rate A_s of stripe cells was set to 50 Hz, and the standard deviation σ_s of each stripe field Gaussian tuning was set to 7% of the stripe spacing (see equation (A 4)). The development of the entorhinal map cells into their adult counterparts was accomplished by using 30 trials, in each of which the animal ran along a novel realistic trajectory of approximately 10 min in a 100×100 cm environment. These trajectories were obtained by rotating an original rat trajectory (data: [13]) about the midpoint of the environment, which is also the starting point, by random angles. In order to ensure that the derived trajectories went beyond the square environment only minimally, the original trajectory was prefixed by a short linear trajectory from the midpoint to the actual starting position at a running speed of 15 cm s^{-1}. The remaining minimal outer excursions were bounded by the environment's limits. The original trajectory was, also, interpolated to increase its temporal resolution to match the time step of numerical integration of model dynamics ($\Delta t = 2$ ms).

To simulate the effects of hippocampal inactivation on learned grid cell responses [91], a trial was run in which ground truth linear velocity values $v(t)$ were additively corrupted by Brownian motion with standard deviation σ_{noise}, and map cells received an extra uniform tonic inhibitory input of A_{off}. Values for σ_{noise} and A_{off} were 3 cm and 5 Hz, respectively.

B.5. Post-processing

The 100×100 cm environment was divided into 2.5×2.5 cm bins. During each trial, the amount of time spent by the animal in the various bins was tracked. Also, for each map cell, the number of spikes generated in the various bins was tracked. At the end of each trial, the resulting occupancy and spike count maps were smoothed using a 5×5 Gaussian kernel with standard deviation equal to unity. Smoothed and unsmoothed spatial rate maps for each map cell were obtained by dividing the corresponding spike count variable by corresponding occupancy variable across the bins. Peak and mean firing rates for a map cell in a given trial were obtained by considering all spatial bins in the corresponding smoothed rate map. Gridness score for each map cell was computed using the method described in [31]. Dynamic (spike-triggered) autocorrelograms for map cells were created by plotting for each spike the relative locations of subsequent spikes that occur within a time window of 10 s [91].

References

1. Morris RGM, Garrud P, Rawlins JNP, O'Keefe J. 1982 Place navigation impaired in rats with hippocampal lesions. *Nature* **297**, 681–683. (doi:10.1038/297681a0)
2. Davis S, Butcher SP, Morris RG. 1992 The NMDA receptor antagonist D-2-amino-5-phosphonopentanoate (D-AP5) impairs spatial learning and LTP *in vivo* at intracerebral concentrations comparable to those that block LTP *in vivo*. *J. Neurosci.* **12**, 21–34.
3. Parron C, Save E. 2004 Evidence for entorhinal and parietal cortices involvement in path integration in the rat. *Exp. Brain Res.* **159**, 349–359. (doi:10.1007/s00221-004-1960-8)
4. O'Keefe J, Dostrovsky J. 1971 The hippocampus as a spatial map. Preliminary evidence from unit activity in the freely-moving rat. *Brain Res.* **34**, 171–175. (doi:10.1016/0006-8993(71)90358-1)
5. Fenton AA, Kao H-Y, Neymotin SA, Olypher A, Vayntrub Y, Lytton WW, Ludvig N. 2008 Unmasking the CA1 ensemble place code by exposures to small and large environments: more place cells and multiple, irregularly arranged, and expanded place fields in the larger space. *J. Neurosci.* **28**, 11 250–11 262. (doi:10.1523/JNEUROSCI.2862-08.2008)
6. Henriksen EJ, Colgin LL, Barnes CA, Witter MP, Moser MB, Moser EI. 2010 Spatial representation along the proximodistal axis of CA1. *Neuron* **68**, 127–137. (doi:10.1016/j.neuron.2010.08.042)
7. Park EH, Dvorak D, Fenton AA. 2011 Ensemble place codes in hippocampus: CA1, CA3, and dentate gyrus place cells have multiple place fields in large environments. *PLoS ONE* **6**, e22349. (doi:10.1371/journal.pone.0022349)
8. Etienne AS, Maurer R, Seguinot V. 1996 Path integration in mammals and its integration with visual landmarks. *J. Exp. Biol.* **199**, 201–209.
9. Gothard KM, Skaggs WE, McNaughton BL. 1996 Dynamics of mismatch correction in the hippocampal ensemble code for space: interaction between path integration and environmental cues. *J. Neurosci.* **16**, 8027–8040.
10. Chen C, King JA, Burgess N, O'Keefe J. 2013 How vision and movement combine in the hippocampal place code. *Proc. Natl Acad. Sci. USA* **110**, 378–383. (doi:10.1073/pnas.1215834110)
11. Hafting T, Fyhn M, Molden S, Moser MB, Moser EI. 2005 Microstructure of a spatial map in the entorhinal cortex. *Nature.* **436**, 801–806. (doi:10.1038/nature03721)
12. McNaughton BL, Battaglia FP, Jensen O, Moser EI, Moser MB. 2006 Path integration and the neural basis of the 'cognitive map'. *Nat. Rev. Neurosci.* **7**, 663–678. (doi:10.1038/nrn1932)
13. Sargolini F, Fyhn M, Hafting T, McNaughton BL, Witter MP, Moser MB, Moser EI. 2006 Conjunctive representation of position, direction, and velocity in entorhinal cortex. *Science* **312**, 758–762. (doi:10.1126/science.1125572)
14. Brun VH, Solstad T, Kjelstrup KB, Fyhn M, Witter MP, Moser EI, Moser MB. 2008 Progressive increase in grid scale from dorsal to ventral medial entorhinal cortex. *Hippocampus* **18**, 1200–1212. (doi:10.1002/hipo.20504)
15. Stensola H, Stensola T, Solstad T, Frøland K, Moser M-B, Moser EI. 2012 The entorhinal grid map is discretized. *Nature* **492**, 72–78. (doi:10.1038/nature11649)
16. O'Keefe J, Burgess N. 2005 Dual phase and rate coding in hippocampal place cells: theoretical significance and relationship to entorhinal grid cells. *Hippocampus* **15**, 853–866. (doi:10.1002/hipo.20115)
17. Gorchetchnikov A, Grossberg S. 2007 Space, time, and learning in the hippocampus: how fine spatial and temporal scales are expanded into population codes for behavioral control? *Neural Netw.* **20**, 182–193. (doi:10.1016/j.neunet.2006.11.007)
18. Rolls ET, Stringer SM, Elliot T. 2006 Entorhinal cortex grid cells can map to hippocampal place cells by competitive learning. *Network* **17**, 447–465. (doi:10.1080/09548980601064846)
19. Molter C, Yamaguchi Y. 2008 Entorhinal theta phase precession sculpts dentate gyrus place fields. *Hippocampus* **18**, 919–930. (doi:10.1002/hipo.20450)
20. Savelli F, Knierim JJ. 2010 Hebbian analysis of the transformation of medial entorhinal grid-cell inputs to hippocampal place fields. *J. Neurophysiol.* **103**, 3167–3183. (doi:10.1152/jn.00932.2009)
21. Grossberg S, Pilly PK. 2012 How entorhinal grid cells may learn multiple spatial scales from a dorsoventral gradient of cell response rates in a self-

organizing map. *PLoS Comput. Biol.* **8**, 31002648. (doi:10.1371/journal.pcbi.1002648.)

22. Mhatre H, Gorchetchnikov A, Grossberg S. 2012 Grid cell hexagonal patterns formed by fast self-organized learning within entorhinal cortex. *Hippocampus* **22**, 320–334. (doi:10.1002/hipo.20901)
23. Pilly PK, Grossberg S. 2012 How do spatial learning and memory occur in the brain? Coordinated learning of entorhinal grid cells and hippocampal place cells. *J. Cogn. Neurosci.* **24**, 1031–1054. (doi:10.1162/jocn_a_00200)
24. Pilly PK, Grossberg S. 2013 How reduction of theta rhythm by medium septum inactivation may disrupt periodic spatial responses of entorhinal grid cells by reduced cholinergic transmission. *Front. Neural Circuits* **7,** 173. (doi:10.3389/fncir.2013.00173)
25. Pilly PK, Grossberg S. 2013 Spiking neurons in a hierarchical self-organizing map model can learn to develop spatial and temporal properties of entorhinal grid cells and hippocampal place cells. *PLoS ONE* **8**, e0060599. (doi:10.1371/journal.pone.0060599)
26. Grossberg S. 1976 Adaptive pattern classification and universal recoding. I. parallel development and coding of neural feature detectors. *Biol. Cybern.* **23**, 121–134. (doi:10.1007/BF00344744)
27. Grossberg S. 1978 A theory of human memory: self-organization and performance of sensory-motor codes, maps, and plans. In *Progress in theoretical biology*, vol. 5 (eds R Rosen, F Snell), pp. 233–374. New York, NY: Academic Press.
28. von der Malsburg C. 1973 Self-organization of orientation sensitive cells in the striate cortex. *Kybernetik* **14**, 85–100. (doi:10.1007/BF00288907)
29. Royer S, Pare D. 2003 Conservation of total synaptic weight through balanced synaptic depression and potentiation. *Nature* **422**, 518–522. (doi:10.1038/nature01530)
30. Langston RF, Ainge JA, Couey JJ, Canto CB, Bjerknes TL, Witter MP, Moser EI, Moser MB. 2010 Development of the spatial representation system in the rat. *Science* **328**, 1576–1580. (doi:10.1126/science.1188210)
31. Wills TJ, Cacucci F, Burgess N, O'Keefe J. 2010 Development of the hippocampal cognitive map in preweanling rats. *Science* **328**, 1573–1576. (doi:10.1126/science.1188224)
32. Olson S, Grossberg S. 1998 A neural network model for the development of simple and complex cell receptive fields within cortical maps of orientation and ocular dominance. *Neural Netw.* **11**, 189–208. (doi:10.1016/S0893-6080(98)00003-3)
33. Grossberg G, Williamson JR. 2001 A neural model of how horizontal and interlaminar connections of visual cortex develop into adult circuits that carry out perceptual groupings and learning. *Cereb. Cortex* **11**, 37–58. (doi:10.1093/cercor/11.1.37)
34. Grossberg S, Seitz A. 2003 Laminar development of receptive fields, maps, and columns in visual cortex: the coordinating role of the subplate. *Cereb. Cortex* **13**, 852–863. (doi:10.1093/cercor/13.8.852)
35. Burgess N, Barry C, O'Keefe J. 2007 An oscillatory interference model of grid cell firing. *Hippocampus* **17**, 801–812. (doi:10.1002/hipo.20327)
36. Hasselmo M, Giocomo L, Zilli E. 2007 Grid cell firing may arise from interference of theta frequency membrane potential oscillations in single neurons. *Hippocampus* **17**, 1252–1271. (doi:10.1002/hipo.20374)
37. Hafting T, Fyhn M, Bonnevie T, Moser MB, Moser EI. 2008 Hippocampus independent phase precession in entorhinal grid cells. *Nature* **453**, 1248–1252. (doi:10.1038/nature06957)
38. Couey JJ *et al*. 2013 Recurrent inhibitory circuitry as a mechanism for grid formation. *Nat. Neurosci.* **16**, 318–324. (doi:10.1038/nn.3310)
39. Pastoll H, Solanka L, van Rossum MC, Nolan MF. 2013 Feedback inhibition enables theta-nested gamma oscillations and grid firing fields. *Neuron* **77**, 141–154. (doi:10.1016/j.neuron.2012.11.032)
40. Cao Y, Grossberg S. 2012 Stereopsis and 3D surface perception by spiking neurons in laminar cortical circuits: a method of converting neural rate models into spiking models. *Neural Netw.* **26**, 75–98. (doi:10.1016/j.neunet.2011.10.010)
41. Giocomo LM, Zilli E, Fransen E, Hasselmo ME. 2007 Temporal frequency of subthreshold oscillations scales with entorhinal grid cell field spacing. *Science* **315**, 1719–1722. (doi:10.1126/science.1139207)
42. Garden DLF, Dodson PD, O'Donnell C, White MD, Nolan MF. 2008 Tuning of synaptic integration in the medial entorhinal cortex to the organization of grid cell firing fields. *Neuron* **60**, 875–889. (doi:10.1016/j.neuron.2008.10.044)
43. Giocomo LM, Hasselmo ME. 2008*b* Time constants of h current in layer II stellate cells differ along the dorsal to ventral axis of medial entorhinal cortex. *J. Neurosci.* **28**, 9414–9425. (doi:10.1523/jneurosci.3196-08.2008)
44. Yoshida M, Giocomo LM, Boardman I, Hasselmo ME. 2011 Frequency of subthreshold oscillations at different membrane potential voltages in neurons at different anatomical positions on the dorsoventral axis in the rat medial entorhinal cortex. *J. Neurosci.* **31**, 12 683–12 694. (doi:10.1523/JNEUROSCI.1654-11.2011)
45. Giocomo LM, Hussaini SA, Zheng F, Kandel ER, Moser MB, Moser EI. 2011 Grid cells use HCN1 channels for spatial scaling. *Cell* **147**, 1159–1170. (doi:10.1016/j.cell.2011.08.051)
46. Boehlen A, Heinemann U, Erchova I. 2010 The range of intrinsic frequencies represented by medial entorhinal cortex stellate cells extends with age. *J. Neurosci.* **30**, 4585–4589. (doi:10.1523/jneurosci.4939-09.2010)
47. Navratilova Z, Giocomo LM, Fellous JM, Hasselmo ME, McNaughton BL. 2012 Phase precession and variable spatial scaling in a periodic attractor map model of medial entorhinal grid cells with realistic after-spike dynamics. *Hippocampus* **22**, 772–789. (doi:10.1002/hipo.20939)
48. Grossberg S, Schmajuk NA. 1989 Neural dynamics of adaptive timing and temporal discrimination during associative learning. *Neural Netw.* **2**, 79–102. (doi:10.1016/0893-6080(89)90026-9)
49. Grossberg S, Merrill JWL. 1992 A neural network model of adaptively timed reinforcement learning and hippocampal dynamics. *Cogn. Brain Res.* **1**, 3–38. (doi:10.1016/0926-6410(92)90003-A)
50. Grossberg S, Merrill JWL. 1996 The hippocampus and cerebellum in adaptively timed learning, recognition, and movement. *J. Cogn. Neurosci.* **8**, 257–277. (doi:10.1162/jocn.1996.8.3.257)
51. Smith MC. 1968 CS-US interval and US intensity in classical conditioning of the rabbit's nictitating membrane response. *J. Comp. Physiol. Psychol.* **3**, 679–687. (doi:10.1037/h0026550)
52. Roberts S. 1981 Isolation of an internal clock. *J. Exp. Psychol. Anim. Behav. Process.* **7**, 242–268. (doi:10.1037/0097-7403.7.3.242)
53. Roberts WA, Cheng K, Cohen JS. 1989 Timing light and tone signals in pigeons. *J. Exp. Psychol. Anim. Behav. Process.* **15**, 23–25. (doi:10.1037/0097-7403.15.1.23)
54. Gibson J. 1991 The origins of scalar timing. *Learn. Motiv.* **22**, 3–38. (doi:10.1016/0023-9690(91)90015-Z)
55. MacDonald CJ, Lepage KQ, Eden UT, Eichenbaum H. 2011 Hippocampal 'time cells' bridge the gap in memory for discontiguous events. *Neuron* **71**, 737–749. (doi:10.1016/j.neuron.2011.07.012)
56. Fiala JC, Grossberg S, Bullock D. 1996 Metabotropic glutamate receptor activation in cerebellar Purkinje cells as substrate for adaptive timing of the classically conditioned eye blink response. *J. Neurosci.* **16**, 3760–3774.
57. Brown J, Bullock D, Grossberg S. 1999 How the basal ganglia use parallel excitatory and inhibitory learning pathways to selectively respond to unexpected rewarding cues. *J. Neurosci.* **19**, 10 502–10 511.
58. Hargreaves EL, Rao G, Lee I, Knierim JJ. 2005 Major dissociation between medial and lateral entorhinal input to dorsal hippocampus. *Science* **308**, 1792–1794. (doi:10.1126/science.1110449)
59. Aminoff E, Gronau N, Bar M. 2007 The parahippocampal cortex mediates spatial and nonspatial associations. *Cereb. Cortex* **17**, 1493–1503. (doi:10.1093/cercor/bhl078)
60. Kerr KM, Agster KL, Furtak SC, Burwell RD. 2007 Functional neuroanatomy of the parahippocampal region: the lateral and medial entorhinal areas. *Hippocampus* **17**, 697–708. (doi:10.1002/hipo.20315)
61. Eichenbaum H, Lipton PA. 2008 Towards a functional organization of the medial temporal lobe memory system: role of the parahippocampal and medial entorhinal cortical areas. *Hippocampus* **18**, 1314–1324. (doi:10.1002/hipo.20500)
62. van Strien NM, Cappaert NLM, Witter MP. 2009 The anatomy of memory: an interactive overview of the parahippocampal-hippocampal network. *Nat. Rev. Neurosci.* **10**, 272–282. (doi:10.1038/nrn2614)

63. Tulving E. 1972 Episodic and semantic memory. In *Organization of memory* (eds E Tulving, W Donaldson), pp. 381–402. New York, NY: Academic Press.
64. Tulving E, Thomson DC. 1973 Encoding specificity and retrieval processes in episodic memory. *Psychol. Rev.* **80**, 352–373. (doi:10.1037/h0020071)
65. Ranck Jr JB. 1984 Head-direction cells in the deep cell layers of dorsal presubiculum in freely moving rats. In *Proc. Annual Conference of the Society for Neuroscience, Anaheim, CA*. 10, 599.
66. Taube JS, Muller RU, Ranck Jr JB. 1990 Head-direction cells recorded from the postsubiculum in freely moving rats. I. Description and quantitative analysis. *J. Neurosci.* **10**, 420–435.
67. Blair H, Sharp P. 1995 Anticipatory head direction signals in anterior thalamus: evidence for a thalamocortical circuit that integrates angular head motion to compute head direction. *J. Neurosci.* **15**, 6260–6270.
68. Skaggs WE, Knierim J, Kudrimoti HS, McNaughton BL. 1995 A model of the neural basis of the rat's sense of direction. *Adv. Neural Inf. Process. Syst.* **7**, 173–180.
69. Blair H, Sharp P. 1996 Visual and vestibular influences on head direction cells in the anterior thalamus of the rat. *Behav. Neurosci.* **10**, 643–660. (doi:10.1037/0735-7044.110.4.643)
70. Redish AD, Elga AN, Touretzky DS. 1996 A coupled attractor model of the rodent head direction system. *Netw. Comput. Neural Syst.* **7**, 671–685. (doi:10.1088/0954-898X/7/4/004)
71. Goodridge JP, Touretzky DS. 2000 Modeling attractor deformation in the rodent head-direction system. *J. Neurophysiol.* **83**, 3402–3410.
72. Boucheny C, Brunel N, Arleo A. 2005 A continuous attractor network model without recurrent excitation: maintenance and integration in the head direction cell system. *J. Comput. Neurosci.* **18**, 205–227. (doi:10.1007/s10827-005-6559-y)
73. Song P, Wang XJ. 2005 Angular path integration by moving 'hill of activity': a spiking neuron model without recurrent excitation of the head-direction system. *J. Neurosci.* **25**, 1002–1014. (doi:10.1523/JNEUROSCI.4172-04.2005)
74. Fortenberry B, Gorchetchnikov A, Grossberg S. 2012 Learned integration of visual, vestibular, and motor cues in multiple brain regions computes head direction during visually-guided navigation. *Hippocampus* **22**, 2219–2237. (doi:10.1002/hipo.22040)
75. Krupic J, Burgess N, O'Keefe J. 2012 Neural representations of location composed of spatially periodic bands. *Science* **337**, 853–857. (doi:10.1126/science.1222403)
76. Caballero-Bleda M, Witter MP. 1993 Regional and laminar organization of projections from the presubiculum and parasubiculum to the entorhinal cortex: an anterograde tracing study in the rat. *J. Comp. Neurol.* **328**, 115–129. (doi:10.1002/cne.903280109)
77. Caballero-Bleda M, Witter MP. 1994 Projections from the presubiculum and the parasubiculum to morphologically characterized entorhinal–hippocampal projection neurons in the rat. *Exp. Brain Res.* **101**, 93–108. (doi:10.1007/BF00243220)
78. Blair HT, Gupta KJ, Zhang K. 2008 Conversion of a phase- to a rate-coded position signal by a three-stage model of theta cells, grid cells, and place cells. *Hippocampus* **18**, 1239–1255. (doi:10.1002/hipo.20509)
79. Thompson LT, Best PJ. 1990 Long-term stability of the place-field activity of single units recorded from the dorsal hippocampus of freely behaving rats. *Brain Res.* **509**, 299–308. (doi:10.1016/0006-8993(90)90555-P)
80. Wilson MA, McNaughton BL. 1993 Dynamics of the hippocampal ensemble code for space. *Science* **261**, 1055–1058. (doi:10.1126/science.8351520)
81. Muller RA. 1996 A quarter of a century of place cells. *Neuron* **17**, 813–822. (doi:10.1016/S0896-6273(00)80214-7)
82. Frank LM, Stanley GB, Brown EN. 2004 Hippocampal plasticity across multiple days of exposure to novel environments. *J. Neurosci.* **24**, 7681–7689. (doi:10.1523/JNEUROSCI.1958-04.2004)
83. Grossberg S. 1980 How does a brain build a cognitive code? *Psychol. Rev.* **87**, 1–51. (doi:10.1037/0033-295X.87.1.1)
84. Grossberg S. 2012 Adaptive resonance theory: how a brain learns to consciously attend, learn, and recognize a changing world. *Neural Netw.* **37**, 1–47. (doi:10.1016/j.neunet.2012.09.017)
85. Carpenter GA, Grossberg S. 1987 A massively parallel architecture for a self-organizing neural pattern recognition machine. *Comput. Vision Graph.* **37**, 54–115. (doi:10.1016/S0734-189X(87)80014-2)
86. Raizada R, Grossberg S. 2003 Towards a theory of the laminar architecture of cerebral cortex: computational clues from the visual system. *Cereb. Cortex* **13**, 100–113. (doi:10.1093/cercor/13.1.100)
87. Desimone R. 1998 Visual attention mediated by biased competition in extrastriate visual cortex. *Proc. R. Soc. Lond. B* **353**, 1245–1255. (doi:10.1098/rstb.1998.0280)
88. Kentros CG, Agniotri NT, Streater S, Hawkins RD, Kandel ER. 2004 Increased attention to spatial context increases both place field stability and spatial memory. *Neuron* **42**, 283–295. (doi:10.1016/S0896-6273(04)00192-8)
89. Kentros C, Hargreaves E, Hawkins RD, Kandel ER, Shapiro M, Muller RV. 1998 Abolition of long-term stability of new hippocampal place cell maps by NMDA receptor blockade. *Science* **280**, 2121–2126. (doi:10.1126/science.280.5372.2121)
90. Morris RGM, Frey U. 1997 Hippocampal synaptic plasticity: role in spatial learning or the automatic recording of attended experience? *Proc. R. Soc. Lond. B* **352**, 1489–1503. (doi:10.1098/rstb.1997.0136)
91. Bonnevie T, Dunn B, Fyhn M, Hafting T, Derdikman D, Kubie JL, Roudi Y, Moser EI, Moser M-B. 2013 Grid cells require excitatory drive from the hippocampus. *Nat. Neurosci.* **16**, 309–319. (doi:10.1038/nn.3311)
92. Grossberg S, Versace M. 2008 Spikes, synchrony, and attentive learning by laminar thalamocortical circuits. *Brain Res.* **1218**, 278–312. (doi:10.1016/j.brainres.2008.04.024)
93. Berke JD, Hetrick V, Breck J, Green RW. 2008 Transient 23- to 30-Hz oscillations in mouse hippocampus during exploration of novel environments. *Hippocampus* **18**, 519–529. (doi:10.1002/hipo.20435)
94. Grossberg S. 2009 Beta oscillations and hippocampal place cell learning during exploration of novel environments. *Hippocampus* **19**, 881–885. (doi:10.1002/hipo.20602)
95. Buffalo EA, Fries P, Landman R, Buschman TJ, Desimone R. 2011 Laminar differences in gamma and alpha coherence in the ventral stream. *Proc. Natl Acad. Sci. USA* **108**, 11 262–11 267. (doi:10.1073/pnas.1011284108)
96. Buschman TJ, Miller EK. 2009 Serial, covert shifts of attention during visual search are reflected by the frontal eye fields and correlated with population oscillations. *Neuron* **63**, 386–396. (doi:10.1016/j.neuron.2009.06.020)
97. Vertes RP, Kocsis B. 1997 Brainstem-diencephalo-septohippocampal systems controlling the theta rhythm of the hippocampus. *Neuroscience* **81**, 893–926. (doi:10.1016/S0306-4522(97)00239-X)
98. Tóth K, Borhegyi Z, Freund TF. 1993 Postsynaptic targets of GABAergic hippocampal in the medial septum-diagonal band of broca complex. *J. Neurosci.* **13**, 3712–3724.
99. Wang XJ. 2002 Pacemaker neurons for the theta rhythm and their synchronization in the septohippocampal reciprocal loop. *J. Neurophysiol.* **87**, 889–900.
100. Brandon MP, Bogaard AR, Libby CP, Connerney MA, Gupta K, Hasselmo ME. 2011 Reduction of theta rhythm dissociates grid cell spatial periodicity from directional tuning. *Science* **332**, 595–599. (doi:10.1126/science.1201652)
101. Koenig J, Linder AN, Leutgeb JK, Leutgeb S. 2011 The spatial periodicity of grid cells is not sustained during reduced theta oscillations. *Science* **332**, 592–595. (doi:10.1126/science.1201685)
102. Burak Y, Fiete IR. 2006 Do we understand the emergent dynamics of grid cell activity? *J. Neurosci.* **26**, 9352–9354. (doi:10.1523/JNEUROSCI.2857-06.2006)
103. Fuhs MC, Touretzky DS. 2006 A spin glass model of path integration in rat medial entorhinal cortex. *J. Neurosci.* **26**, 4266–4276. (doi:10.1523/JNEUROSCI.4353-05.2006)
104. Guanella A, Kiper D, Verschure P. 2007 A model of grid cells based on a twisted torus topology. *Int. J. Neural Syst.* **17**, 231–240. (doi:10.1142/S0129065707001093)
105. Burgess N. 2008 Grid cells and theta as oscillatory interference. Theory and predictions. *Hippocampus* **18**, 1157–1174. (doi:10.1002/hipo.20518)
106. Zilli EA. 2012 Models of grid cell spatial firing published 2005–2011. *Front. Neural Circuits* **6**, 16. (doi:10.3389/fncir.2012.00016)

107. Kropff E, Treves A. 2008 The emergence of grid cells: intelligent design or just adaptation? *Hippocampus* **18**, 1256–1269. (doi:10.1002/hipo.20520)
108. Fyhn M, Hafting T, Treves A, Moser MB, Moser EI. 2007 Hippocampal remapping and grid realignment in entorhinal cortex. *Nature* **446**, 190–194. (doi:10.1038/nature05601)
109. Yartsev MM, Witter MP, Ulanovsky N. 2011 Grid cells without theta oscillations in the entorhinal cortex of bats. *Nature* **479**, 103–107. (doi:10.1038/nature10583)
110. Domnisoru C, Kinkhabwala AA, Tank DW. 2013 Membrane potential dynamics of grid cells. *Nature* **495**, 199–204. (doi:10.1038/nature11973)
111. Schmidt-Heiber C, Hausser M. 2013 Cellular mechanisms of spatial navigation in the medial entorhinal cortex. *Nat. Neurosci.* **16**, 325–331. (doi:10.1038/nn.3340)
112. Muzzio IA, Levita L, Kulkami J, Monaco J, Kentros C, Stead M, Abbott LF, Kandel ER. 2009 Attention enhances the retrieval and stability of visuospatial and olfactory representations in the dorsal hippocampus. *PLoS Biol.* **7**, e1000140. (doi:10.1371/journal.pbio.1000140)
113. Gaudiano P, Grossberg S. 1991 Vector associative maps: unsupervised real-time error-based learning and control of movement trajectories. *Neural Netw.* **4**, 147–183. (doi:10.1016/0893-6080(91)90002-M)